GLOBAL BIOGEOCHEMICAL CYCLES, VOL. 12, NO. 1, PAGES 1–24, MARCH 1998

Evaluation of terrestrial carbon cycle models through simulations of the seasonal cycle of atmospheric CO_2: First results of a model intercomparison study

M. Heimann,[1] G. Esser,[2] A. Haxeltine,[3] J. Kaduk,[1,8] D. W. Kicklighter,[4] W. Knorr,[1] G. H. Kohlmaier,[5] A. D. McGuire,[6] J. Melillo,[4] B. Moore III,[7] R. D. Otto,[5] I. C. Prentice,[3] W. Sauf,[1] A. Schloss,[7] S. Sitch,[3,9] U. Wittenberg,[2] and G. Würth [5]

Abstract. Results of an intercomparison among terrestrial biogeochemical models (TBMs) are reported, in which one diagnostic and five prognostic models have been run with the same long-term climate forcing. Monthly fields of net ecosystem production (NEP), which is the difference between net primary production (NPP) and heterotrophic respiration R_H, at 0.5° resolution have been generated for the terrestrial biosphere. The monthly estimates of NEP in conjunction with seasonal CO_2 flux fields generated by the seasonal Hamburg Model of the Oceanic Carbon Cycle (HAMOCC3) and fossil fuel source fields were subsequently coupled to the three-dimensional atmospheric tracer transport model TM2 forced by observed winds. The resulting simulated seasonal signal of the atmospheric CO_2 concentration extracted at the grid cells corresponding to the locations of 27 background monitoring stations of the National Oceanic and Atmospheric Administration/Climate Monitoring and Diagnostics Laboratory network is compared with measurements from these sites. The Simple Diagnostic Biosphere Model (SDBM1), which is tuned to the atmospheric CO_2 concentration at five monitoring stations in the northern hemisphere, successfully reproduced the seasonal signal of CO_2 at the other monitoring stations. The SDBM1 simulations confirm that the north-south gradient in the amplitude of the atmospheric CO_2 signal results from the greater northern hemisphere land area and the more pronounced seasonality of radiation and temperature in higher latitudes. In southern latitudes, ocean-atmosphere gas exchange plays an important role in determining the seasonal signal of CO_2. Most of the five prognostic models (i.e., models driven by climatic inputs) included in the intercomparison predict in the northern hemisphere a reasonably accurate seasonal cycle in terms of amplitude and, to some extent, also with respect to phase. In the tropics, however, the prognostic models generally tend to overpredict the net seasonal exchanges and stronger seasonal cycles than indicated by the diagnostic model and by observations. The differences from the observed seasonal signal of CO_2 may be caused by shortcomings in the phenology algorithms of the prognostic models or by not properly considering the effects of land use and vegetation fires on CO_2 fluxes between the atmosphere and terrestrial biosphere.

[1] Max-Planck-Institut für Meteorologie, Hamburg, Germany.
[2] Institut für Pflanzenökologie, Justus-Liebig-Universität, Giessen, Germany.
[3] Global Systems Group, Department of Ecology, University of Lund, Lund, Sweden.
[4] The Ecosystems Center, Marine Biological Laboratory, Woods Hole, Massachusetts.
[5] Institut für Physikalische und Theoretische Chemie, J. W. Goethe-Universität, Frankfurt, Germany.
[6] Alaska Cooperative Fish and Wildlife Research Unit, National Biological Service, University of Alaska, Fairbanks.
[7] Center for Complex Systems, Institute for the Study of Earth, Oceans, and Space, University of New Hampshire, Durham.
[8] Now at Department of Plant Biology, Carnegie Institution of Washington, Stanford, California.
[9] Now at Potsdam Institute for Climate Impact Research, Potsdam, Germany

Paper number 97GB01936.
0886-6236/98/97GB-01936$12.00

1. Introduction

The terrestrial biosphere takes up an amount of CO_2 equivalent to about one sixth of the total atmospheric inventory every year [see, e.g., *Schimel*, 1995]. This carbon flux into the biosphere represents gross primary production (GPP), that is, carbon fixed in photosynthesis (and not rapidly released in photorespiration) by terrestrial plants. About half of GPP is returned to the atmosphere as plant (autotrophic) respiration. The remainder represents net primary production (NPP), that is, carbon that accrues to the growth of plants.

In the absence of disturbance and major climatic fluctuations, annual net primary production (NPP_{year}) is believed to be almost in balance with annual heterotrophic respiration ($R_{H,year}$) by soil microorganisms, so that annual net ecosystem production (NEP_{year}), which represents the net exchange between the terrestrial biosphere and the atmosphere (NEP = NPP - R_H), is relatively small. However, the rates of photosynthesis and detritus/soil organic matter decomposition are under the control of different envi-

ronmental factors that are not synchronized during the seasonal cycle. On a weekly or monthly basis, NEP can therefore fluctuate over a large range of positive or negative values. Positive NEP (i.e., NPP > R_H) indicates a terrestrial sink for atmospheric CO_2, whereas negative NEP (i.e., NPP < R_H) indicates a terrestrial source for atmospheric CO_2. This seasonal fluctuation of NEP is primarily responsible for the observed seasonal variations in atmospheric CO_2 content, especially at high northern latitudes where these variations have the greatest amplitude [*Fung et al.*, 1983, 1987, *Heimann et al.*, 1989]. The role played by land-atmosphere fluxes in causing these seasonal variations is graphically demonstrated by "flying carpet" diagrams that show the contrast in magnitude and a 180° phase difference between the cycles in the northern and southern hemispheres and phase plots that show annually repeated hysteresis patterns in the relation between satellite-derived "greenness" (as normalized-difference vegetation index (NDVI)) and detrended atmospheric CO_2 concentrations in the northern and tropical latitude bands [*Fung et al.*, 1987].

Recognition of the terrestrial biosphere's key role in the global carbon cycle has prompted the development of several models to quantify the metabolism of terrestrial ecosystems at a global scale. Such models are of two main types: diagnostic models, which use weekly to monthly remote sensing data such as composites of the normalized-difference vegetation index (NDVI) as input, and prognostic models, which use only environmental (climate and soil) data as input. The first diagnostic terrestrial biosphere (or biogeochemical) models (TBMs) expressed NPP as a simple function of incident photosynthetically active radiation (PAR) and NDVI [*Fung et al.*, 1987; *Heimann and Keeling*, 1989]. More recent models take into account more mechanistic aspects of primary production, including the constraints on the light use efficiency of evergreen vegetation imposed by low temperatures and drought [*Potter et al.*, 1993; *Ruimy et al.*, 1994]. The first prognostic models expressed NPP as an empirical function of annual characteristics of climate (e.g., temperature, precipitation, and evapotranspiration [*Lieth*, 1975]); again, more recent models include more mechanistic representations of processes including explicit simulation of vegetation foliage cover and phenology as responses to the environment. Thus the two types of models are converging, and some current models can be run in either diagnostic or prognostic mode according to whether the seasonal variations in foliage cover are predicted or prescribed.

Global TBMs are multiplying rapidly, as shown by recent publications [e.g., *Raich et al.*, 1991; *Melillo et al.*, 1993; *Potter et al.*, 1993; *Foley*, 1994; *Lüdeke et al.*, 1994; *Ruimy et al.*, 1994; *Warnant et al.*, 1994; *Friend*, 1995; *Woodward et al.*, 1995; *VEMAP Members*, 1995; *Kaduk and Heimann*, 1996]. The models are still quite diverse in their structure (for example, in whether nitrogen cycling is treated as an active pathway controlling NPP or as passive consequence of a system driven by light and water); quantitative functions (there is a wide range of values used for key parameters, such as the temperature dependence of respiration); and results (models differ considerably in simulated spatial patterns and seasonality of NPP as well as in their simulated values for total global NPP, even when forced by identical inputs (Potsdam 1994/1995 workshops, [*Lurin et al.*, 1994])). The existence of such differences indicates a need for evaluation to discriminate among different formulations. However, so far, relatively little effort has been put into evaluating the performance of TBMs. Field-based NPP measurements represent a minimal benchmark. However, they are imprecise, and being related to specific points in space and time, they reflect strongly the local weather and soil characteristics at the time of measurement. Thus they do not directly test the large-scale aggregated flux computations that are more important for the model's applications to the global carbon cycle.

An alternative approach is provided by the available time series of CO_2 measurements in the remote atmosphere, which offer an appropriately large spatial scale for evaluating the aggregated carbon fluxes simulated by TBMs. The CO_2 measurement data give a clear picture of the seasonal cycles, latitudinal gradients, interannual variability, and (increasingly) stable isotope composition of atmospheric CO_2 [*Keeling et al.*, 1989, 1995; *Conway et al.*, 1994a], all of which are in principle predictable by TBMs. However, such comparisons are complicated by the need to specify in addition fossil fuel emissions and to model not only the terrestrial biosphere-atmosphere carbon exchanges but also the corresponding ocean-atmosphere exchanges and the three-dimensional transport of CO_2 by winds from the atmospheric and oceanic exchange sites to the remote measurement sites. A rigorous evaluation thus requires that the TBMs are linked to accurate representations of fossil fuel CO_2 emissions, ocean-atmosphere seasonal CO_2 fluxes, and atmospheric tracer transport [*Heimann et al.*, 1989]. Despite the fact that neither of these additional factors is known at present to sufficient accuracy, the approach, nevertheless, provides a consistent framework within which to assess some aspects of large-scale carbon fluxes as simulated by TBMs.

This paper focuses on mean seasonal cycles of atmospheric CO_2 concentration, as recorded at 27 background monitoring stations of the National Oceanic and Atmospheric Administration/Climate Monitoring and Diagnostic Laboratory (NOAA/CMDL) flask sampling network [*Conway et al.*, 1994a] covering all the major climatic zones of the earth. It describes the results of a TBM intercomparison in which six TBMs (one diagnostic and five prognostic models) have been run under similar protocols on a 0.5° grid (55.6 x 55.6 km^2 at the equator). Each TBM was run to equilibrium for each grid element; that is, the annual totals of NPP and R_H are equal ($NPP_{year} = R_{H,year}$). As a consequence, the NEP_{year} estimates of the TBMs are not appropriate for examining the spatial pattern of the anthropogenically induced terrestrial sink for atmospheric CO_2 believed to be operating today [*Schimel et al.*, 1995]. However, the temporal NEP estimates are useful for simulating the seasonal dynamics of CO_2 throughout the biosphere. The spatially explicit monthly results of the TBMs (NPP and R_H), combined with equivalent seasonal CO_2 flux fields generated by the Hamburg Model of the Oceanic Carbon Cycle (HAMOCC3) [*Maier-Reimer*, 1993, *Six and Maier-Reimer*, 1996] and fossil fuel source fields derived from standard sources [*Marland et al.*, 1989], have been used to provide the lower boundary condition to a three-dimensional tracer transport model (TM2) forced by observed winds (Figure 1). The seasonal cycles at locations corresponding to the sampling stations have been extracted and compared with the (detrended) measurements at each station. The objective was to determine the extent to which different models can simulate the observed seasonal cycles and latitudinal patterns.

2. Model Descriptions

2.1. Ocean Model

Monthly fluxes of CO_2 between the atmosphere and the surface layer of the ocean were obtained from a standard run of the Hamburg Model of the Ocean Carbon Cycle (HAMOCC3) [*Maier-Re-*

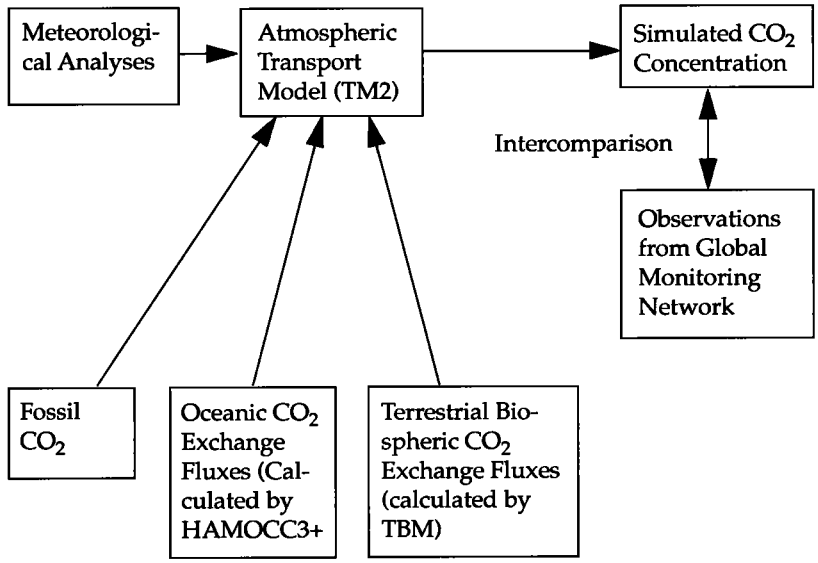

Figure 1. Flowchart of the data flow and and the model links.

imer, 1993] enhanced with a recently developed model of the marine biosphere [*Kurz*, 1993; *Six and Maier-Reimer*, 1996]. The ocean carbon cycle model is embedded in the global three-dimensional, seasonal flow field of the Hamburg Large-Scale Geostrophic ocean circulation model (LSG) [*Maier-Reimer et al.*, 1993]. HAMOCC3 describes the cycling of oceanic carbon in its three inorganic forms on a three-dimensional grid with a horizontal resolution of approximately 3.5° and 12 layers in the vertical dimension. The marine biosphere is described in the model by two organic carbon pools which represent phytoplankton and zooplankton. Gas exchange at the surface is computed in the model by the air-sea difference in partial pressure of CO_2 (pCO_2) multiplied by a wind speed and temperature dependent gas exchange formulation according to *Liss and Merlivat* [1986], scaled to satisfy the constraint imposed by the global bomb radiocarbon balance [*Heimann and Monfray*, 1989].

In this study we employed monthly net sea-to-air fluxes of CO_2 as calculated by a steady state run of HAMOCC3 with a prescribed, constant atmospheric CO_2 concentration. The model computed pCO_2 fields, which are the major driving force for the seasonal air-sea exchange flux of CO_2, show a fair agreement with observational time series and regional survey data [*Kurz*, 1993]. Furthermore, an alternative validation based on the seasonal cycle of oxygen in the atmosphere also confirms that the model-calculated effects of the marine biosphere on the ocean carbon system are reasonably well simulated, at least in the southern hemisphere [*Kurz*, 1993; *Six and Maier-Reimer*, 1996].

2.2. Atmospheric Transport Model

The three-dimensional atmospheric transport model used in this study is the TM2 model [*Heimann*, 1995], representing a further development of the TM1 model used in numerous previous atmospheric CO_2 simulation studies [e.g. *Heimann and Keeling*, 1989; *Heimann et al.*, 1989] and which originated from the Goddard Institute for Space Studies tracer model [*Russell and Lerner*, 1981]. TM2 solves the continuity equation of an atmospheric constituent on a three-dimensional Eulerian grid spanning the whole globe. The standard coarse grid resolution employed in this study is approximately 7.83° latitude by 10° longitude and nine layers in the vertical dimension. Tracer transport is described in the model by means of specified three-dimensional time-varying wind fields and by a vertical transport parametrization representing vertical mixing by cumulus clouds and by turbulent diffusion. The meteorological wind fields used in the simulation experiments are based on 12-hourly analyses of the European Centre for Medium-Range Weather Forecasts for the year 1987.

There exist quite a few approaches to model atmospheric transport, and a recent intercomparison among global transport models [*Law et al.*, 1996] revealed substantial differences in the concentration fields computed from the same prescribed surface sources by different transport models. The TM2 model in many respects performed close to the "typical" coarse-grid transport model [*Law et al.*, 1996]. Clearly, an assessment of the sensitivity of the present results with respect to atmospheric transport, for example, by making use of different transport models, would be worthwhile but is beyond the scope of the present paper.

For the simulation experiments described below, each source was prescribed as a seasonally varying surface flux and the transport models was run for 4 years until the modeled atmospheric CO_2 concentration reached an approximatly cyclo-stationary state. The results of the fourth year were used in the subsequent analysis.

2.3. Terrestrial Biosphere Models

Six global terrestrial biogeochemical models were examined in this intercomparison study: the BIOME2 model, the Frankfurt Biosphere Model (FBM), the High-Resolution Biosphere Model (HRBM), the Simple Diagnostic Biosphere Model (SDBM1), the Simulating Land Vegetation and NPP Model (SILVAN), and the Terrestrial Ecosystem Model (TEM). Although all these models simulate the exchange of carbon between atmosphere and terrestrial biosphere, they use different approaches for the calculation of NPP. The diagnostic model included in this study (SDBM1) uses monthly NDVI data to estimate absorbed radiation which is then translated into NPP through an efficiency coefficient. In contrast,

the five prognostic models either calculate NPP directly from statistical relations between temperature and precipitation which is then modified as functions of soil characteristics (HRBM), or they estimate NPP as the difference between GPP and autotrophic respiration (BIOME2, FBM, SILVAN, and TEM). In HRBM, SDBM1, and TEM, climate data enter into the flux calculations as monthly means, while BIOME2, FBM, and SILVAN apply simple algorithms to interpolate to daily values from the monthly climate data and determine fluxes on a daily time step. All models consider carbon and water cycling, but the TEM also includes nitrogen dynamics. Among the TBMs, phytomass is represented by different numbers of carbon pools (BIOME2, 3; FBM, 2; HRBM, 4; SDBM1, 0; SILVAN, 3; and TEM, 1). Gross photosynthesis (GPP) is either calculated with a multiple limitation approach (FBM and TEM) or by modified versions of the Farquhar model [*Farquhar et al.*, 1980] (BIOME2 and SILVAN). Although R_H in all models is calculated by relationships that depend on soil carbon, temperature, and soil moisture, either the formulations of the relationships or the parameters of similar formulations differ among the models.

The brief model descriptions given in the following subsections 2.3.1. to 2.3.6. will concentrate on the historic development and the main features and assumptions of each model that determine the computation of the CO_2 exchange fluxes on the seasonal timescale. A short model comparison is given in Table 1; more detailed information can be found in the references cited at the beginning of each subsection.

2.3.1. BIOME2. BIOME2 [*Haxeltine et al.*, 1996, *Haxeltine and Prentice*, 1996] is a coupled carbon and water-flux simulation model that has been designed for use in predicting the response of global natural vegetation to changing climates. Thus the model does not use a map of global vegetation as a forcing data set but instead predicts global vegetation patterns as a model output. The BIOME2 has a simple two-layer hydrology model which allows a realistic simulation of the drought stress experienced by vegetation and a mechanistic carbon balance model. Model output consists of predictions of NPP, leaf area index, and vegetation type, which is the combination of plant types which maximizes whole ecosystem net primary production (NPP) at a particular site. Woody and grass plant types are differentiated according to their physiological and phenological attributes and rooting strategies.

The modeling approach has been to produce a mechanistic model of natural ecosystems which, nevertheless, has a level of complexity appropriate for use at the global scale with monthly climate data. The monthly climate fields are linearly interpolated yielding quasi-daily values for use in the water-flux model [*Haxeltine et al.*, 1996].

Photosynthesis is calculated using a semimechanistic light use efficiency (LUE) model. The LUE model is basically an optimized version of the Farquhar photosynthesis model [*Collatz et al.*, 1991, 1992]. Instead of prescribing values for the parameter V_m (the maximum catalytic capacity of the enzyme "ribulose biphosphate carboxylase oxygenase" per unit leaf area), an optimal value for V_m given a particular vegetation type (C3 or C4 plants) and set of environmental conditions is calculated. The result is an equation for photosynthesis which is linearly dependent on absorbed photosynthetically active radiation (APAR) such that

$$\mathrm{GPP}_{\max} = \mathrm{FPC} f_1(\mathrm{CO}_2, T, d)\ \mathrm{APAR} \quad (1)$$

where $\mathrm{GPP}_{\max}$ is the potential or "maximum possible" GPP, $f_1(\mathrm{CO}_2,T,d)$ represents the semimechanistic LUE equation which depends on temperature (T), ambient carbon dioxide concentration (CO_2) and the day length (d). Foliar projected cover (FPC) is the variable used to define leaf area in BIOME2. It is measured as the fraction of ground covered by foliage vertically above it (i.e., values ranging from 0-1). FPC is calculated from one-sided leaf area index (LAI) using Beer's law [*Monsi and Saeki*, 1953]:

$$\mathrm{FPC} = 1 - e^{-\mathrm{LAI}/2} \quad (2)$$

An optimal value of FPC is predicted for each model grid square, and this optimal value of FPC is used in the final NPP calculation.

The potential GPP is then reduced by a scalar in order to take into account the effects of drought stress (Φ_D) and temperature extremes (Φ_T):

$$\mathrm{GPP} = \mathrm{GPP}_{\max}\, \Phi_D\, \Phi_T \quad (3)$$

Finally, net primary production is calculated by subtracting whole plant respiration costs, which are currently estimated as being 50% of $\mathrm{GPP}_{\max}$.

Heterotrophic respiration (R_H) is calculated from a relationship derived by *Lloyd and Taylor* [1994] and *Howard and Howard* [1993], where CO_2 evolution is related to both monthly soil temperature and average monthly soil moisture content. Monthly soil temperature was derived from air temperature assuming an attenuation factor and a phase lag computed by the propagation of an annual heat wave through soil [*Campbell* 1977]. R_H is calculated using the following relationship:

$$R_H = \alpha\, f_2(T_{soil}) f_3(w_{soil}) \quad (4)$$

where w_{soil} is the soil moisture. The value α can be regarded as the product of the soil decay rate, which is dependent on the soil type, and the mass of soil carbon. An initial estimate of α was subsequently scaled such that the steady state constraint condition ($\mathrm{NPP}_{\mathrm{year}} = R_{H,\mathrm{year}}$) was satisfied. Thus, monthly heterotrophic respiration estimates were obtained. This method avoids the need to explicitly define the various soil decay rates and also the need for estimating the soil carbon content.

2.3.2. Frankfurt Biosphere Model (FBM). The FBM [*Kindermann et al.*, 1993; *Lüdeke et al.*, 1994; *Kohlmaier et al.*, 1997] consists of a mechanistic carbon model and a simple one-layer bucket model for soil moisture. Litter and soil organic carbon are combined in one soil compartment. Vegetation is represented by two compartments to which assimilated carbon is allocated by an allometric relation. Model output includes daily carbon exchange fluxes, leaf area, phytomass and soil carbon.

The two vegetation compartments are green carbon compartment (GC) comprising leaves and feeder roots with a lifetime of up to about 4 years and a residual carbon compartment (RC) which includes the carbon mass stored in branches, stem, and roots. The dynamics of all three carbon compartments result from the daily input and output fluxes as follows:

1. Carbon assimilation (GPP) is calculated using a factorial approach in which a vegetation type specific maximum assimilation rate ($\mathrm{GPP}_{\max}$) is multiplied by different factors for the dependence on leaf area index (LAI) (calculated from leaf mass and a vegetation type dependent specific leaf area), incident photosynthetic active radiation (PAR), air temperature (T), the ratio of actual to potential evapotranspiration (AET/PET), and atmospheric CO_2 concentration

$$\mathrm{GPP} = \mathrm{GPP}_{\max} f_4(\mathrm{PAR}, \mathrm{LAI}) f_5(T) \frac{\mathrm{AET}}{\mathrm{PET}} f_6(\mathrm{CO}_2) \quad (5)$$

Table 1. Comparison of Biogeochemical Processes and Compartments Among the Terrestrial Biosphere Models

Process	BIOME2	FBM 2.2	HRBM 3.0	SBDM1	SILVAN 2.2	TEM 4.0
Evapotranspiration	Priestly-Taylor, reduction by soil moisture	*Thornthwaite and Mather* [1957], reduction by soil moisture	*Prentice et al.* [1992]	equilibrium ET [*McNaughton and Jarvis*, 1983], ET max. 1mm/hour at field capacity	*Federer* [1982]	*Jensen and Haise* [1963]
Number of soil water layers	2	1	1	1	1	1
Carbon uptake by vegetation	Farquhar-Collatz with optimized V_{max} and soil moisture limitation	multiple limitation GPP	potential or actual NPP	Monteith with water-stress factor	AET/PET *f(T,I,CO_2,O_2), f = simplified Farquhar model	multiple limitation GPP
Leaf area index (LAI)	optimized	leaf phytomass × SLA	diagnostic from green phytomass	FPAR derived from NDVI	leaf phytomass × SLA	not explicitly calculated
$C_i = f(C_a)$	yes	$C_i = 0.7C_a$, C_3 plants $C_i = 0.4C_a$, C_4 plants	no → implicit	no	$C_i = 0.7C_a$, C_3 plants $C_i = 0.4C_a$, C_4 plants	yes
Plant respiration Q_{10}	Arrhenius type dependence	1.5	NA	NA	0.5 - 2.0 at 15 °C	1.5 - 2.5
Decomposition	*Lloyd and Taylor* [1994]	*Fung et al.* [1987] + f(AET/PET), Q_{10} = 1.5 - 2.0	empirical function for temperature and humidity (Q_{10} regionally different)	Q_{10} = 1.5	empirical function for temperature and humidity [*Esser* 1991]	Q_{10} = 2.0
Number of vegetation carbon pools	3	2	4	0	3	1
Number of litter / soil carbon pools	1	1	5	0	3	1
Nitrogen uptake by vegetation	NA	NA	considered in version 5.0 [*Nevison et al.*, 1996]	NA	NA	monthly
Net nitrogen mineralization (NMIN)	NA	NA	full dynamic system in version 5.0	NA	NA	mineralization/immobilization dynamics
Number of vegetation nitrogen pools	NA	NA	NA	NA	NA	2
Number of litter / soil nitrogen pools	NA	NA	NA	NA	NA	2
Temporal scale	monthly (for C-balance), quasi-daily (for water-balance)	daily/hourly	monthly	monthly	daily to monthly	monthly
			Global Annual Results, Pg C			
NPP_{year}	56.6	50.3	46.4	60.0	61.0	49.0
GPP_{year}	NA	147.2	NA	NA	119.0	137.0
$R_{H,year}$	56.6	50.3	46.4	60.0	61.0	49.0

C_a, atmospheric CO_2 concentration; C_i, internal leaf CO_2 concentration; NPP_{year}, annual net primary production; and SLA, specific leaf area. NA indicates not available.

2. Autotrophic respiration from *GC* and *RC* which depends on compartment size and an exponential function of temperature with a constant Q_{10} value specified for each vegetation type.

3. Litter production (*LP*) is proportional to the compartment size with a constant coefficient except for the *GC* compartment of deciduous vegetation which will shed the leaves within about 1 month.

4. Heterotrophic respiration (R_H) uses the temperature dependence of *Fung et al.* [1987], linear dependence on compartment size, and a soil moisture factor analogous to the moisture dependence of photosynthesis.

The phenological behavior of the model is governed by a set of rules for carbon partitioning of evergreen and deciduous vegetation types. The leaf shooting phase starts when the carbon gain from photosynthesis is greater than the carbon losses. The system allocates most of the assimilates to the *GC* compartment until *GC* corresponds to *RC* as defined by an allometric relation [*Janecek et al.*, 1989]

$$RC = a\,GC^b \tag{6}$$

(with a and b dependent on vegetation type), which states that a minimum amount of *RC* is required to support a given mass of leaves and feeder roots. During the secondary growth phase the system is forced to allocate simultaneously into the *GC* and *RC* compartments in such a way that (6) remains valid. The end of the vegetation period is defined by unfavorable weather conditions which result in biomass decrease.

For deciduous vegetation types a leaf abscission phase follows in which the *GC* compartment is reduced to a residual amount which is defined by the function

$$RC = c\,GC^d \tag{7}$$

(with c and d dependent on vegetation type). In the following dormancy phase the carbon losses (litter production and autotrophic respiration) are distributed among the compartments so that (7) remains valid.

For evergreen vegetation types the vegetation period is followed by a standby phase in which the losses of *GC* and *RC* are characterized by constant proportions. All flux equations contain free parameters which are determined through calibration for a steady state such that the mean annual gross and net primary productivity and heterotrophic respiration of a vegetation type equal average ecological estimates. The model requires hourly values of temperature and radiation as well as daily precipitation and a variety of static data about vegetation and soil. Daily precipitation is obtained from the monthly values by means of a smooth redistribution. In a similar way the monthly mean temperature and mean cloudiness are interpolated to daily values. The hourly values of temperature are generated with the help of a sinusoidal function using independent estimates of daily temperature range for each vegetation type. The percentage cloudiness is constant over the day, and the diurnal cycle of radiation is calculated using the Ångström relationship.

It is then possible to calculate the seasonal courses of LAI, phytomass, GPP, NPP, and R_H in a steady state ($NPP_{year} = LP_{year} = R_{H,year}$) as well as the long-term development of nonclimax vegetation.

An application of the FBM to different climate scenarios for the northern forest biomes is described by *Lüdeke et al.* [1995] and the validation of the model-predicted phenology using NDVI data is given in *Lüdeke et al.* [1996].

2.3.3. High-Resolution Biosphere Model (HRBM). The HRBM is the successor of the Osnabrück Biosphere Model [*Esser*, 1987, 1991]. It represents the biosphere by nine carbon pools and in its version 3.0 includes modules dealing with vegetation fires and human influences through land use changes and emissions from fossil fuel and from industry. A detailed description is given by *Esser et al.* [1994].

The nine biospheric carbon pools are herbaceous and woody live phytomass, litter from herbaceous and woody material (dead phytomass), and soil organic carbon, with the live and dead phytomass pools subdivided into aboveground and belowground pools. The biospheric fluxes are net primary productivity (NPP), litter production (*LP*), soil organic carbon production and heterotrophic respiration (R_H). NPP is calculated individually for each of the four compartments of live phytomass.

In the HRBM, empirical models are used to calculate annual net primary production (NPP_{year}) [*Esser*, 1987, 1991] and litter production (LP_{year}) [*Esser*, 1991], which are seasonally distributed afterward. The distribution of NPP_{year} follows monthly actual evapotranspiration (AET), which is derived from a simple bucket model [*Prentice et al.*, 1992]. The distribution of LP_{year} from herbaceous phytomass follows the relative decrease of AET between 2 months. In biomes with seasonal litter fall ("temperate deciduous," "cool mixed," "cold mixed," "cold deciduous," and "tundra"), litter production starts when monthly air temperature drops to half of the mean monthly temperature of the warmest month (on the centigrade scale) and reduces the herbaceous phytomass by half within 14 days. In contrast, the litter production coefficient from woody phytomass is assumed to be 1/12 of the annual value each month.

The litter decomposition flux is proportional to the size of the litter pool. The value of the coefficient depends on the composition of the litter material and on climate. While decomposition increases exponentially with air temperature, the dependence on precipitation is a skewed maximum function with an initial steep decomposition increase with increasing precipitation followed by a slower decrease in decomposition at high precipitation rates. The maximum decomposition rate is also dependent on temperature: higher temperatures shift the maximum decomposition to higher precipitation rates.

The primary factors that control seasonal CO_2 exchanges between the biosphere and the atmosphere are the seasonal air temperature and precipitation signal which affect monthly NPP, *LP*, and decomposition. In this intercomparison experiment the modules that refer to land use and vegetation fires have not been considered.

2.3.4. Simple Diagnostic Biosphere Model (SDBM1). The SDBM1 [*Knorr and Heimann*, 1995] is a simple, diagnostic, globally uniform model of monthly CO_2 exchange between the atmosphere and the terrestrial biosphere. Modeled NPP and R_H are computed from remote sensing and climate data. The model version employed in this study is the formulation I described in the *Knorr and Heimann* [1995] work, in which both NPP and R_H depend also on water stress computed using a simple bucket model.

Carbon uptake by vegetation (NPP) is calculated from estimates of photosynthetically active radiation (PAR) absorbed by vegetation, which is determined from a combination of bi-weekly maxima of the normalized-difference vegetation index (NDVI) of the NOAA 9 satellite (1985-1989) [*Gallo*, 1992] and cloudiness data, regridded from the original mercator projection grid (approximately 10' resolution at the equator) to the 0.5°x0.5° standard latitude-

longitude model grid. A one-layer bucket model calculates water stress as the ratio between actual and potential evapotranspiration (AET/PET) from monthly means of precipitation, temperature, and cloudiness.

Specifically, NPP is calculated from

$$\mathrm{NPP} = \alpha\ 1.222\left(\frac{\mathrm{NDVI}}{0.559} - 0.1566\right)\frac{\mathrm{AET}}{\mathrm{PET}}\,\mathrm{PAR} \qquad (8)$$

where PAR is assumed to be half of mean monthly global radiation at the surface [W m^{-2}]. Carbon release from soils is assumed to depend on relative evapotranspiration and exponentially on air temperature, T, with no cutoff at low freezing temperatures

$$R_H = \beta\, Q_{10}^{\,T/10}\left(\frac{\mathrm{AET}}{\mathrm{PET}}\right) \qquad (9)$$

α and Q_{10} are globally uniform parameters determined from fitting the model-derived seasonal cycle to atmospheric CO_2 observations from five key stations in the northern hemisphere, selected to cover approximately uniformly the major regions in temperate latitudes with strongly seasonal vegetation ($Q_{10} = 1.5$ and $\alpha = 0.68$ gC (MJ PAR)$^{-1}$). The value of the parameter β is not globally uniform, but is determined from the condition of equilibrium ($\mathrm{NPP}_{\mathrm{year}} = R_{H,\mathrm{year}}$).

2.3.5. Simulating Land Vegetation and NPP Model (SILVAN). SILVAN [*Kaduk and Heimann*, 1996, *Kaduk*, 1996] consists of a mechanistic carbon model and a simple one-layer bucket model for the estimation of the water balance. The biosphere is represented by three pools of living biomass (assimilates, herbaceous, and woody phytomass) and three pools of dead biomass (herbaceous and woody litter and soil organic carbon). Model output includes daily exchange fluxes of carbon, LAI (single sided), biomass, and soil carbon.

The assimilate pool represents carbohydrates serving as reserves for the plants. Herbaceous biomass includes leaves and fine roots, woody biomass sapwood, and heartwood of stems and roots. Fixed fractions of the herbaceous and woody carbon pools are considered as belowground carbon. Leaf area index is linearly related to aboveground herbaceous carbon and constrained by growing conditions and the diagnostically computed sapwood cross-sectional area.

Assimilation at the leaf level is simulated by applying a simplified version of the photosynthesis model of *Farquhar et al.* [1980]. Leaf assimilation is then scaled to the canopy with the current leaf area index and a fixed light extinction coefficient of k = 0.5. Integrating the diurnal cycle of temperature and PAR results in nonwater-stressed daily assimilation. This rate is then adjusted by the ratio of actual to potential evapotranspiration.

Assimilated carbon is stored in the assimilate pool and used for respiration and growth. Maintenance and growth respiration are simulated for leaf, fine root, and sapwood compartments. Maintenance respiration rates are tied to the maximal assimilation rate. The temperature dependence of maintenance respiration is simulated by an Arrhenius relationship adjusted to be equivalent to a Q_{10} of 2 at the optimal temperature for net assimilation.

Growth, starting with bud burst, is triggered in tropical biomes when production conditions are good, that is, when drought stress is low (AET/PET>0.4). Thus the model does not impose any dormancy for the tropical vegetation, hence which may respond instantaneously to improved weather conditions. In temperate biomes, growth begins when the growing degree day temperature sum exceeds a certain threshold depending on chilling days and the biome. (The growing degree day sum is defined by the sum of the mean daily temperatures above 5°C since December 1 for the northern and June 1 for the southern hemispheres.) Relations of this type have been shown to describe the date of bud burst in temperate biomes rather well [*Murray et al.*, 1989]. The biome dependent parameter values in the formulae have been determined by an evaluation of satellite data. In contrast to tropical vegetation this modeling approach implies a dormancy period for the temperate vegetation, since growth only starts after the temperature sum exceeds a threshold.

The allocation strategy employed in SILVAN aims at maximization of NPP. Allocation of carbon is directed from the assimilate pool to the leaves until an optimal LAI is reached. This optimal LAI is defined by resulting in maximal NPP given the current environmental conditions and current plant state. Further assimilates are allocated to wood according to an allometric relation of sapwood and LAI as long as this leads to an increase in NPP thereby increasing the potential LAI that the vegetation can support with water by increasing sapwood cross-sectional area. Excess assimilates are directed to dead structural wood.

No a priori limits are imposed on the simulated LAI. Typical mean annual LAI for a grid cell (biome average) ranges from 0.2 to 3.8 depending on the biome. Intrabiome variation is typically low because of similar climate and constant biological parameter values.

In all biomes a low continuous leaf mortality is in effect at all times, mimicking herbivore consumption and decay of photosynthetic potential throughout the growing season. Beyond this base mortality rate, leaf and fine root shedding in tropical biomes follows the production conditions; that is, if AET/PET > 0.4 and the current LAI is higher than the optimal LAI estimated for the time step, a fraction of the excess herbaceous biomass is shed. If AET/PET<0.4, then all herbaceous biomass is shed within 2 weeks. In temperature biomes, shedding of herbaceous biomass is initiated when daily minimum temperature drops below 0°C and it is assumed to last 1 month. Woody litter production proceeds with a fixed rate throughout the whole year.

Finally, litter decomposition rates are modeled by empirical functions depending on temperature and precipitation as in previous versions of the HRBM [*Esser*, 1991]; heterotrophic respiration is the product of the rates and current pool sizes.

In summary, SILVAN features a fully climate-driven phenology using simple empirical functions which are based on results from field experiments. Note that in SILVAN phenology and allocation are not only crucial for production but also for heterotrophic respiration, as they determine timing and amount of litter production.

2.3.6. Terrestrial Ecosystem Model (TEM). The Terrestrial Ecosystem Model (TEM) is described in detail by *Raich et al.* [1991], *McGuire et al.* [1992, 1993, 1995, 1997], and *Melillo et al.* [1993]. To date, TEM has been used to examine patterns of NPP for potential vegetation in South America [*Raich et al.*, 1991] and North America [*McGuire et al.*, 1992] and to examine the potential response of NPP and carbon storage to climate change [*McGuire et al.*, 1993, 1995, 1996, 1997; *Melillo et al.*, 1993, 1995; *Joyce et al.*, 1995]. In this study we use version 4.0 of TEM [*McGuire et al.*, 1995].

The TEM is a process-based ecosystem simulation model that uses spatially explicit data on climate, soil texture, vegetation, and water availability to make monthly estimates of important carbon and nitrogen fluxes and pool sizes. The TEM is a highly aggregated model in which terrestrial ecosystems are represented by one veg-

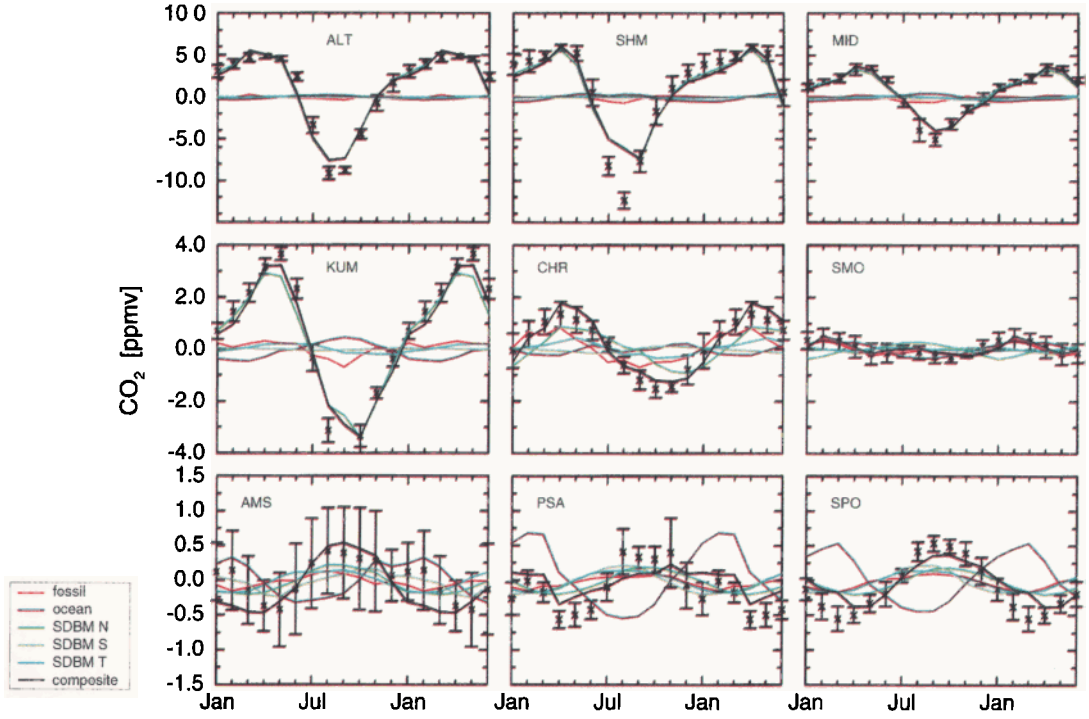

Plate 1. Comparison of the observed seasonal cycle of CO_2 at nine selected monitoring stations with the simulated seasonal cycle produced by coupling the monthly estimates of net ecosystem production by the Simple Diagnostic Biosphere Model (SDBM1) and fossil fuel emissions with the Hamburg ocean and atmospheric transport models. SDBM1 N, SDBM S, and SDBM T denote the contributions from NEP north of 30°N, south of 30°S and from the tropics (30°S-30°N), respectively. Mean and standard deviation are shown for the seasonal cycle derived from the NOAA data set [*Conway et al.*, 1994] as described in the text. The first 6 months of each cycle are displayed twice to reveal the annual variation more clearly.

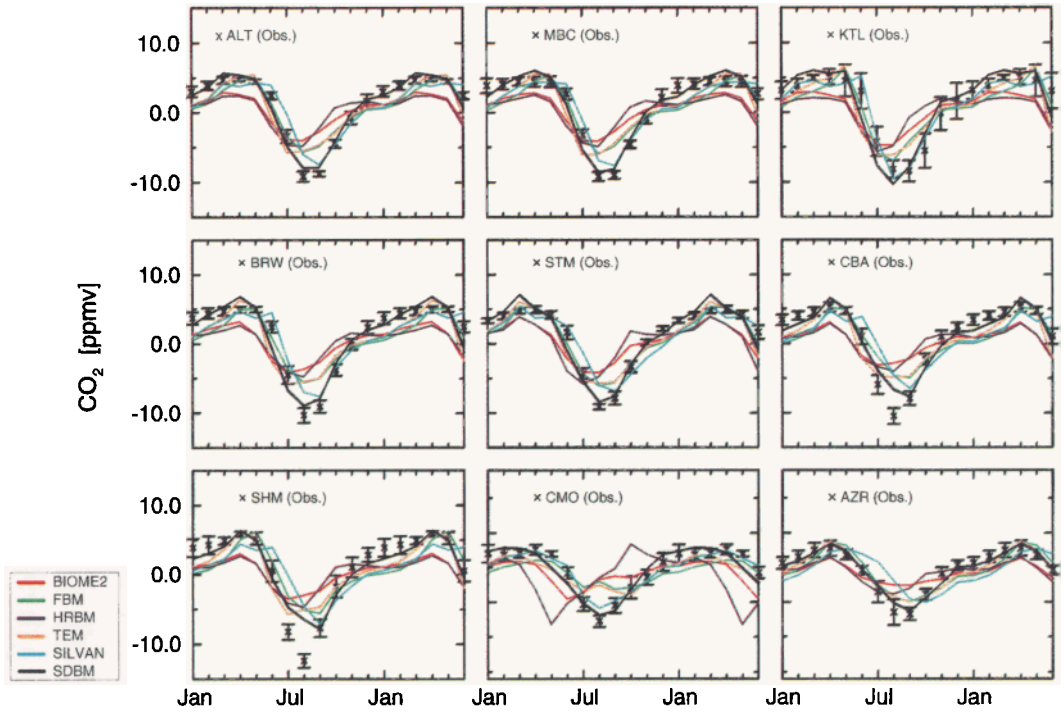

Plate 2a. Comparison of the observed seasonal cycle of CO_2 with the simulated seasonal cycle produced by coupling the monthly estimates of net ecosystem production by the six terrestrial biosphere models (TBMs) and fossil fuel emissions with the Hamburg ocean and atmospheric transport models for northern monitoring stations. The first 6 months of each cycle are displayed twice to reveal the annual variation more clearly. Mean and standard deviations are shown for the observed data.

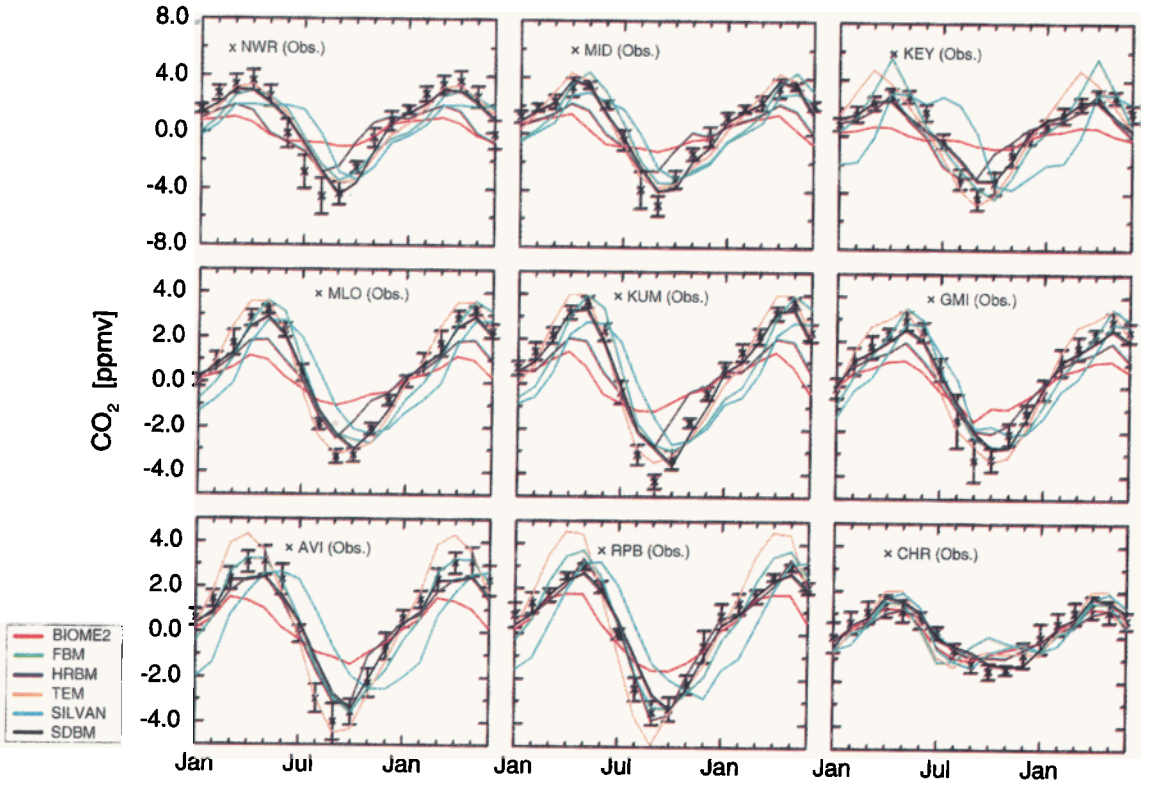

Plate 2b. As in Plate 2a but for tropical monitoring stations.

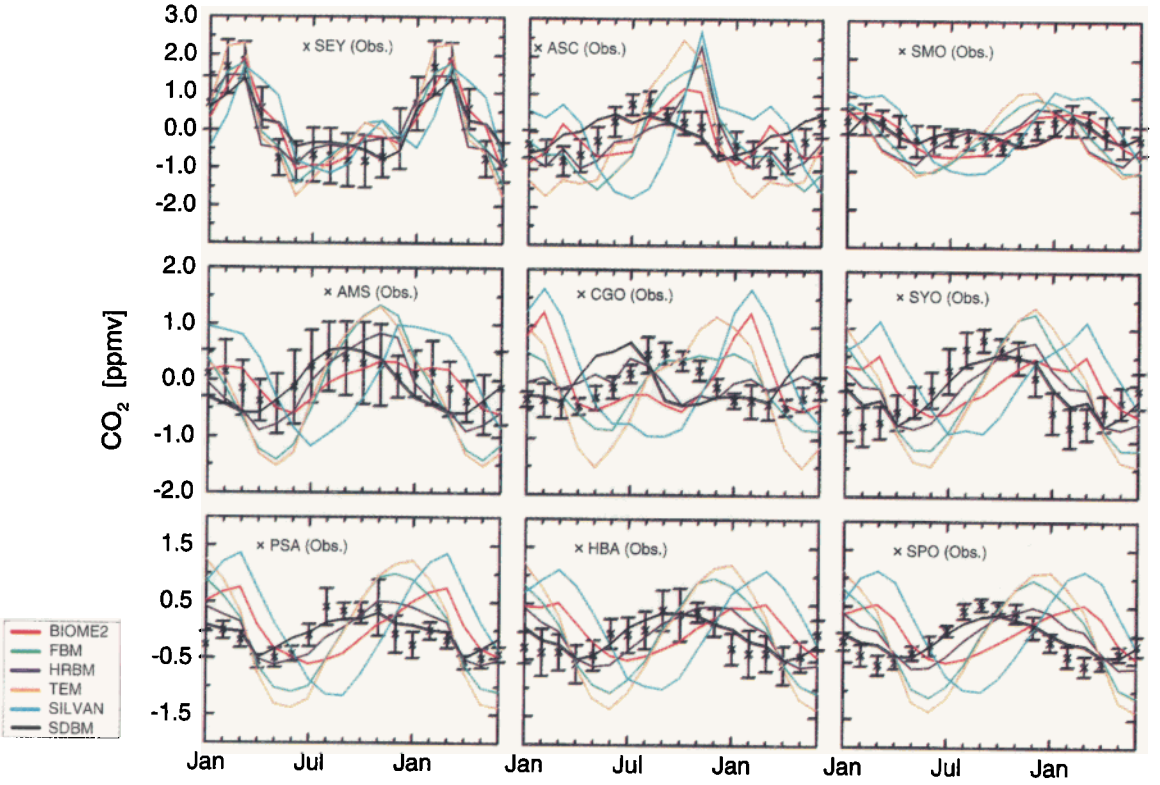

Plate 2c. As in Plate 2a but for southern monitoring stations.

etation carbon pool, two vegetation nitrogen pools (structural and labile), one soil organic carbon pool, and two soil nitrogen pools (organic and inorganic). Hydrology for TEM is determined by the water balance model of *Vörösmarty et al.*, [1989].

Parameters in TEM are vegetation-specific, soil-specific, or constant. The vegetation used by TEM in this study is an updated version of the vegetation given by *Melillo et al.* [1993]. Although most of the vegetation-specific parameters are defined either from the literature or from statistical analyses of data, the rate-limiting parameters in most flux equations are determined by calibration. The calibration of these parameters is one technique for addressing issues of temporal and spatial scale in the model [see *Rastetter et al.*, 1992]. In TEM the rate-limiting parameters are determined by calibrating the model so that it estimates the equilibrium fluxes and pools of an intensively studied field site, that is, the calibration site for the vegetation type. Data used to calibrate the rate-limiting parameters of version 4.0 are documented in Table 1 of *McGuire et al.* [1995].

The seasonality of carbon exchange between the terrestrial biosphere and the atmosphere is influenced by differences in the seasonality of NPP and R_H. In TEM, NPP is calculated as the difference between GPP and plant respiration. A number of factors influence the seasonality of GPP, which is calculated monthly as follows

$$\mathrm{GPP} = \mathrm{GPP_{max}}\ \mathrm{LEAF}\ f_7(\mathrm{PAR})\, f_8(T)\, f_9(\mathrm{CO_2}, \mathrm{H_2O})\, f_{10}(NA) \quad (10)$$

where $\mathrm{GPP_{max}}$ is the maximum rate of C assimilation, PAR is photosynthetically active radiation, LEAF is leaf area relative to maximum leaf area, T is monthly mean air temperature, CO_2 is the atmospheric concentration of carbon dioxide, H_2O is water availability, and NA is nitrogen availability. The parameter $\mathrm{GPP_{max}}$ is the rate-limiting parameter in the GPP equation and is determined by calibration. Of the several functions in the GPP equation, LEAF plays a major role in the controlling the seasonality of C assimilation. This function simulates relative changes in the photosynthetic capacity of mature vegetation from estimated actual evapotranspiration and the previous month's photosynthetic capacity [*Raich et al.*, 1991]:

$$\mathrm{LEAF_j} = a(\mathrm{EET_j}/\mathrm{EET_{max}}) + b(\mathrm{LEAF_{j-1}}) + c \quad (11)$$

where $\mathrm{LEAF_j}$ is the relative leaf phenology in the current month j, $\mathrm{EET_j}$ is the estimated actual evapotranspiration in the current month, $\mathrm{EET_{max}}$ is the maximum monthly evapotranspiration, and $\mathrm{LEAF_{j-1}}$ is relative leaf phenology in the previous month. Note that LEAF is constrained to be between 1.0 and a minimum relative leaf phenology. The parameters a, b, and c are vegetation-specific parameters [see *McGuire et al.*, 1992] that are determined by regressing the relative leaf phenology of the current month with $\mathrm{EET}/\mathrm{EET_{max}}$ and the previous month's leaf phenology for a site with seasonal data on leaf area. Relative leaf phenology is calculated as the ratio of leaf area index in the current month to the maximum monthly leaf area index.

The functions f_7, f_8, f_9, and f_{10} also influence the seasonality of C assimilation. The function f_7(PAR) describes the effect of photosynthetically active radiation on C assimilation. Because f_7 is a scalar function that increases hyperbolically from 0 to 1 as PAR increases [see *Raich et al.*, 1991], it tends to increase GPP more during months with greater solar radiation at the top of the canopy.

The function $f_8(T)$ describes the effects of air temperature on C assimilation. This function increases parabolically from 0 to 1 between the minimum and optimum temperature of photosynthesis [see *Raich et al.*, 1991] and remains at 1 until it reaches the maximum temperature of photosynthesis where it decreases parabolically to 0 [see *McGuire et al.*, 1995]. The minimum and maximum temperatures of photosynthesis are vegetation-specific parameters that are defined by the growing season limits of the vegetation type [see *McGuire et al.*, 1995]. The optimum temperature of photosynthesis is grid-cell-specific and is defined as the month of maximum relative leaf phenology for the grid cell [see *McGuire et al.*, 1995]. Thus f_8 tends to increase GPP most during months when the temperature exceeds the temperature of the month with maximum leaf area.

The function $f_9(\mathrm{CO_2},\mathrm{H_2O})$ describes the simultaneous effects of atmospheric CO_2 and water availability on C assimilation. This function calculates a scalar that increases hyperbolically from 0 to 1 as the intercellular concentration of CO_2 increases [see *Raich et al.*, 1991]. Intercellular CO_2 is the product of atmospheric CO_2 and relative canopy conductance, which is approximately a linear function of the ratio of actual estimated evapotranspiration to potential evapotranspiration (EET/PET) [see *Raich et al.*, 1991; *McGuire et al.*, 1992]. Because the seasonal variation of atmospheric CO_2 is a small fraction of the atmospheric CO_2 concentration, the seasonality of f_9 is primarily determined by the seasonality of EET/PET, which is highest in wet months and lowest in dry months.

The function $f_{10}(NA)$ describes how carbon-nitrogen status of the vegetation, i.e., nitrogen availability or supply, influences carbon assimilation. Nitrogen supply is the sum of nitrogen uptake plus nitrogen mobilized from the vegetation labile nitrogen pool [*McGuire et al.*, 1993]. Nitrogen supply is generally greatest early in the growing season when vegetation is able to mobilize nitrogen from storage. Nitrogen uptake depends on temperature, soil moisture, and inorganic nitrogen in the soil solution [see *Raich et al.*, 1991] and increases for higher air temperature, higher soil moisture, and higher inorganic nitrogen. Net nitrogen mineralization, which depends in part on decomposition, replenishes inorganic nitrogen, and tends to be greater for higher air temperature and higher soil moisture. Thus, the seasonality of f_{10} is influenced by the dynamics of vegetation nitrogen storage, nitrogen uptake, and nitrogen mineralization.

In TEM, the calculation of plant respiration considers both maintenance and construction respiration. Maintenance respiration (R_m) is calculated as follows:

$$R_m = K_r\, C_v\, e^{r_T T} \quad (12)$$

where K_r is the per-gram respiration rate of vegetation biomass at 0°C, C_V is the mass of carbon in the vegetation, T is the mean monthly air temperature, and r_T is the instantaneous rate of change in respiration with air temperature. The parameter K_r is the rate-limiting parameter in the R_m equation and is determined by calibration. The parameter r_T is equal to $\ln(Q_{10})/10$ where Q_{10} is the rate of change of respiration due to a 10°C increase in temperature. In TEM, Q_{10} is modeled as follows [see *McGuire et al.*, 1992]:

$$Q_{10} = 2.35665 + 0.05308\, T + 0.00238\, T^2 - 0.00004\, T^4 \quad (13)$$

where T is mean monthly air temperature. This function approximates a linear increase in Q_{10} from 1.5 to 2.0 between 40° and 20°C, a constant Q_{10} of 2 between 20° and 5°C, and a linear increase in Q_{10} from 2.0 to 2.5 between 5° and 0°C [see *Larcher*, 1980]. The seasonality of R_m is determined primarily by the seasonality in T and secondarily by the seasonality in C_V. The season-

ality of construction respiration, which is calculated as 20% of the difference between GPP and R_m, depends on the relative seasonality of GPP and R_m.

A number of factors influence the seasonality of R_H, which is calculated as follows:

$$R_H = K_d \ \text{SOC} \ f_{11}(T) \ f_{12}(S_m) \quad (14)$$

where K_d is the per-gram respiration rate ofsoil organic carbon (SOC) at 0°C, T is mean monthly air temperature, and S_m is volumetric soil moisture. The parameter K_d is the rate-limiting parameter in the R_H equation and is determined by calibration. The seasonality of R_H is primarily determined by the seasonality of f_{11} and f_{12}. The function $f_{11}(T)$ describes the effect of mean monthly air temperature on heterotrophic respiration and is modeled as an exponential function of T with a Q_{10} of 2.0. Thus the seasonality of f_{11} depends on the seasonality of air temperature. The function $f_{12}(S_m)$ describes the effect of soil moisture on decomposition, which is a parabolic relationship that depends on volumetric soil moisture and has an optimum at approximately field capacity. Thus the seasonality of f_{12} depends on the seasonality of soil moisture.

3. Data

3.1. Input Data for the TBMs

An equilibrium run was performed for each of the six terrestrial biosphere models under a prescribed atmospheric CO_2 concentration of 340 parts per million by volume (ppmv). All of the models used the same 0.5°x0.5° horizontal grid. The climate used to drive the models is based on the precipitation, temperature, and cloudiness data sets of Cramer and Leemans [W. Cramer, *personal communication, 1994*], which is an updated version of the *Leemans and Cramer* [1991] database. These data are long-term average monthly mean values and are given on a 0.5° grid for the entire land surface (without Antarctica). If necessary, the monthly values were interpolated to daily and hourly timesteps using simple interpolation schemes and periodic functions as described in section 2.3.

All fluxes are calculated for potential vegetation (disregarding human influences) except for the SDBM1 which implicitly includes land use through its application of satellite data (NDVI). The descriptions of the pattern of vegetation types (biomes) and soil characteristics (soil type and texture) are different in each model, though all soil data layers used here are based on the FAO soil map of the world [Food and Agriculture Organization, 1971-1979]. Vegetation distribution is either taken from observation-based maps or derived from climate (BIOME2, HRBM, and SILVAN, see sections 2.3.1, 2.3.3, 2.3.5.).

3.2. Observations of the Atmospheric CO_2 Concentration

Atmospheric observations of the CO_2 concentration used in the present study were obtained from the comprehensive monitoring program of the National Oceanographic and Atmospheric Administration. This network consists of approximately 30 stations covering latitudes from 82°N to 90°S, with the highest density of stations in the Americas, in Antarctica, and on Pacific islands and the biggest gaps over the Eurasian and African continents [*Conway et al.*, 1994a]. We used the monthly averaged station data provided by the Carbon Dioxide Information and Analysis Center [*Conway et al.*, 1994b].

For each station record the following procedure was used to extract the seasonal cycle of atmospheric CO_2 from the station records. First, a smooth continuous representation of the interannual CO_2 concentration trend was obtained by interpolating the annual mean concentrations with Hermite cubics. Thereby the needed first derivatives of the trend function at the center of each year were estimated by centered differences from the annual mean concentrations of the adjacent years. Second, trend-corrected monthly concentration values were calculated by subtracting the interannual CO_2 trend function from the monthly observations. Third, monthly estimates of the seasonal cycle and of its variability were obtained by computing average and 1 standard deviation of all trend-corrected January, February, etc., values within the time window 1983-1992. The standard deviations reflect the interannual variability of the seasonal cycle within the selected time window. A total of 27 stations from the NOAA network contained sufficiently long records to perform this procedure (Figure 2). A list of the selected stations is given in Table 2.

3.3. CO_2 Source From Fossil Fuel Burning

The component in the atmospheric CO_2 concentration resulting from the release of CO_2 from fossil fuel burning and cement manufacture was computed based on a global 1°x1° map compiled by *Marland et al.* [1989]. Fossil fuel CO_2 emissions were assumed to be constant in time during each year. In several regions of the globe this is probably not the case: indeed, *Rotty* [1987] determined a seasonality in the northern hemisphere of 18%, while *Levin et al.*, [1989], based on ^{14}C measurements, inferred an even larger seasonality in northern Europe. It is expected that fossil fuel use for heating in winter (in higher latitudes) and for cooling in summer (in lower latitudes) induces a seasonal release pattern. However, these sources typically contribute only about one third to the total industrial CO_2 emissions, which themselves are substantially smaller than the seasonal fluxes of interest in this study. On the basis of these considerations we do not expect the assumption of constant industrial CO_2 emissions to significantly affect the modeled results.

4. Results

To evaluate how well a simulation reproduced the observed seasonal signal of atmospheric CO_2 at a monitoring station, we calculated a normalized mean-squared deviation (NMSD) defined as

$$\text{NMSD} = \frac{1}{12} \sum_{m=1}^{12} \left(\frac{C_{T,m} + C_{F,m} + C_{O,m} - C_{OBS,m}}{\sigma_m} \right)^2 \quad (15)$$

where $C_{T,m}$, $C_{F,m}$, and $C_{O,m}$ are the monthly CO_2 concentrations resulting from the corresponding biospheric, fossil fuel, and ocean flux, respectively, $C_{OBS,m}$ is the 10-year-mean observed value (1983-1992), and σ_m is the corresponding standard deviation of the observed value for each month (m=1,...,12) of the year. The resulting NMSDs of the TBMs for each of 27 monitoring stations are documented in Table 3.

4.1. Comparisons to CO_2 Monitoring Stations: The Simple Diagnostic Biosphere Model

The Simple Diagnostic Biosphere Model (SDBM1) is a diagnostic tool that was designed to help examine temporal patterns of

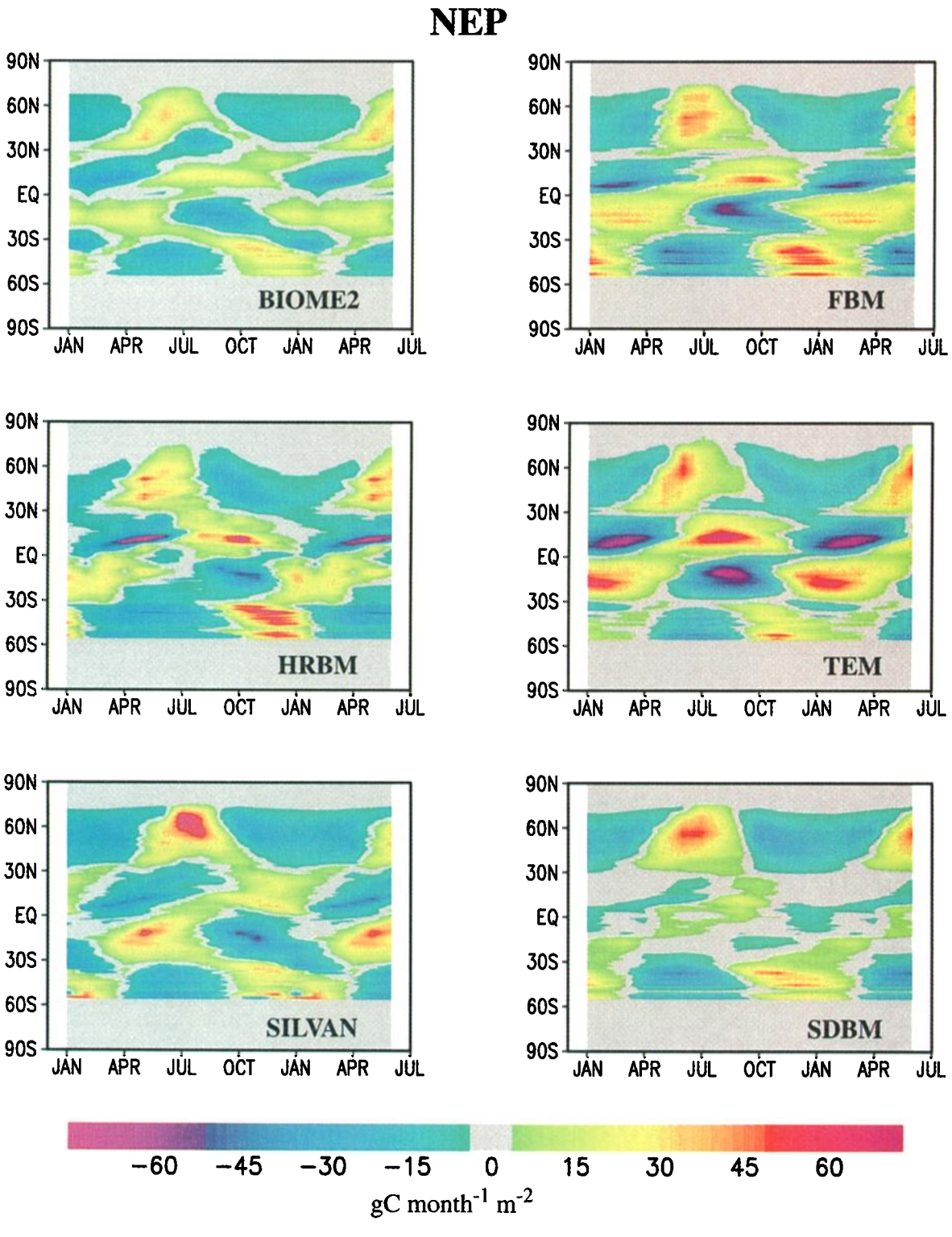

Plate 3a. Zonally averaged net ecosystem production (NEP) for each of the terrestrial biosphere models shown versus latitude and time of the year. Units are in g C $month^{-1}$ m^{-2} of land area in the terrestrial biosphere.

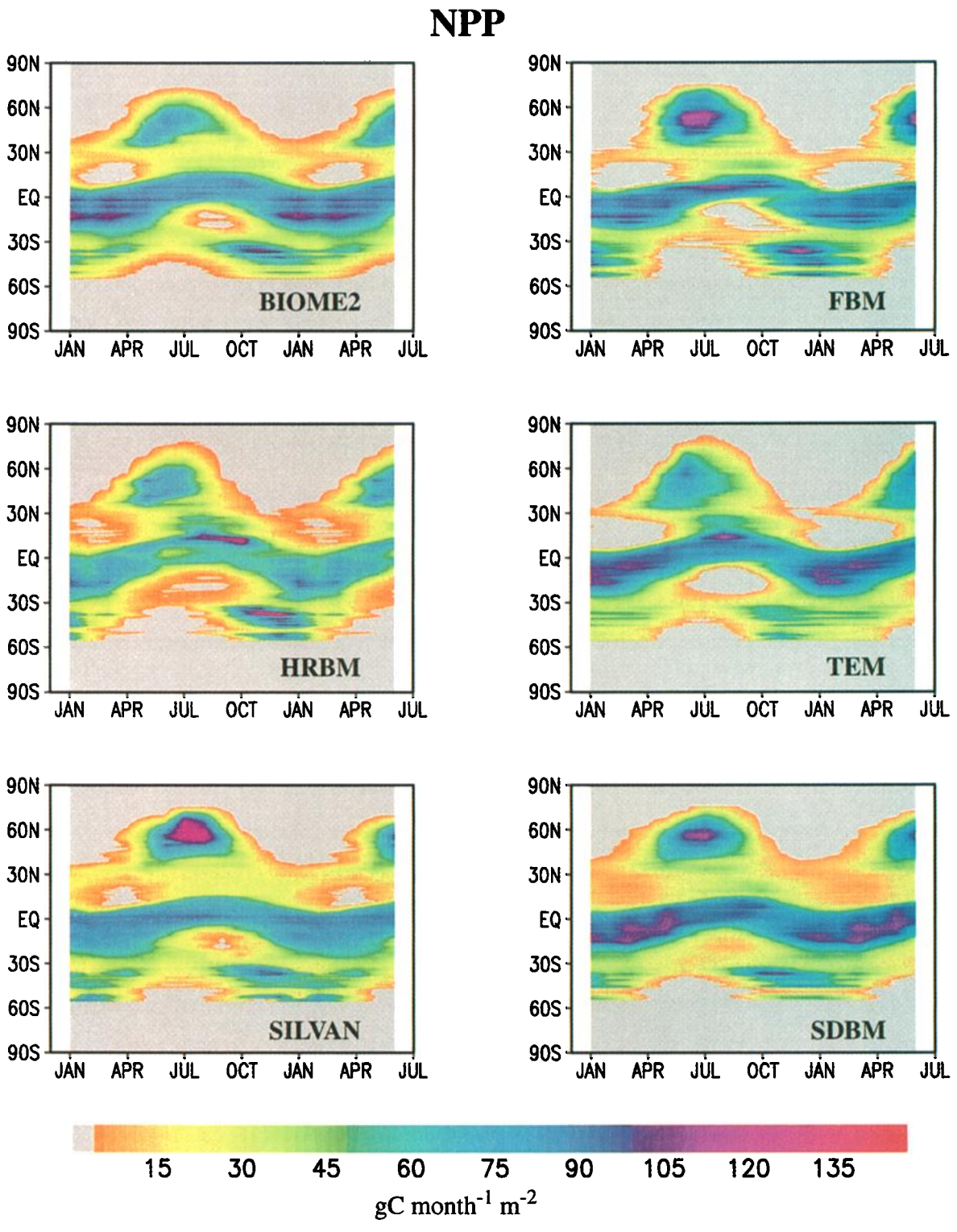

Plate 3b. As in Plate 3a but for net primary production (NPP).

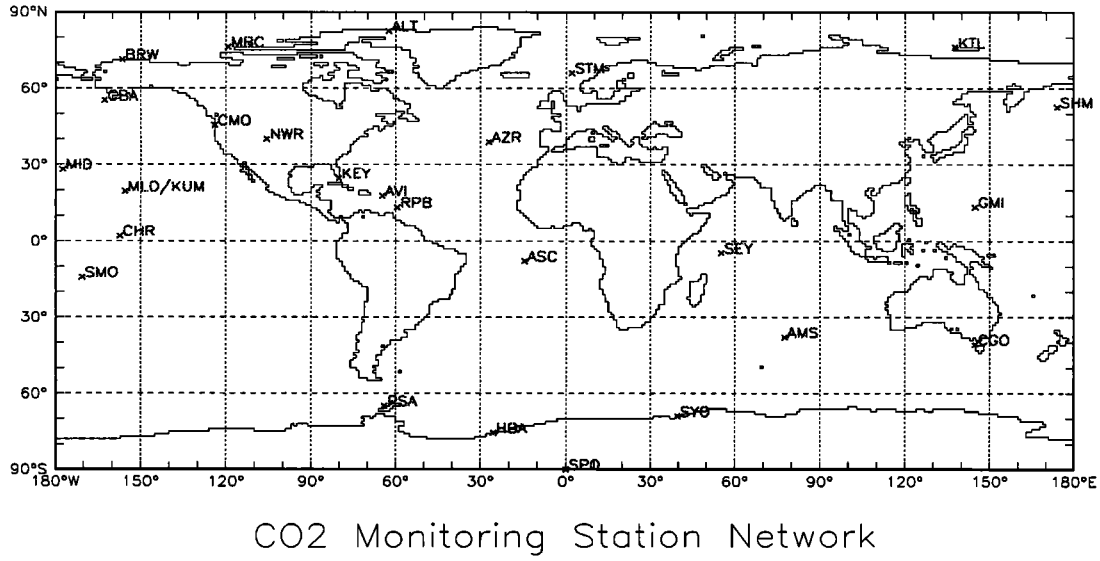

Figure 2. Locations of the 27 CO_2 monitoring stations considered in this study [*Conway et al.*, 1994b]. The two solid lines delineate the middle and high-latitude northern, tropical (30°S - 30°N) and midlatitude southern source regions from which the contributions to the seasonal station signals were computed with the Simple Diagnostic Biosphere Model (SDBM1) (see Plate 1).

sources and sinks of CO_2 throughout the terrestrial biosphere. The global parameters in the NPP (α) and R_H (Q_{10}) relationships of SDBM1 have been calibrated such that the simulated seasonal signal of atmospheric CO_2 represents a good fit to the seasonal signals measured at 5 of the 27 monitoring stations. As described by Knorr and Heimann [1995], the five calibration stations were selected to cover approximately uniformly the major regions in the northern hemisphere temperate latitudes with strongly seasonal vegetation (see Table 2). Not surprisingly, the agreement between the SDBM1 simulations and the observed seasonal signals is good at most stations: the median NMSD among the 27 stations is 1.7 and the range of NMSD is between 0.3 and 8.4 (Table 3). Exceptions are Station "M" (STM), Cold Bay (CBA), Shemya Island (SHM), and Cape Grim (CGO), where the normalized mean-squared deviation (NMSD) is greater than 5 (Table 3). At STM there is close agreement between the model simulations and the observations, but because of the small standard deviation of the observations at this station (approximately 0.5 ppmv), the NMSD is large. At CBA and SHM the simulation differs moderately from the measured signal, especially in June and July. At Cape Grim (CGO) the simulation differs substantially from the observations, which may be attributed in part to the fact that in the transport model the Cape Grim location lies in a grid box with a substantial land surface area, which implies that the simulated signal at the station is largely dominated by the local sources. However, the observations, in order to be representative of southern hemisphere background air, are selected according to wind direction and wind speed. This inconsistency is responsible for a large fraction of the discrepancy at this station [*Ramonet and Monfray*, 1996].

For the terrestrial biosphere the SDBM1 estimates both an annual NPP and an annual R_H of 60.0 Pg C (10^{15} g C). In the context of simulating the seasonal signal of atmospheric CO_2, the temporal pattern of NEP at any spatial scale is more relevant than the absolute values of NPP and R_H; NPP and R_H estimates could be biased either high or low and still produce a good fit to the seasonal signal of CO_2 at the monitoring stations [*Knorr and Heimann*, 1995, Figure 1].

The SDBM1 simulation is useful in identifying the relative contributions of fossil fuel emissions, oceanic CO_2 exchange, and terrestrial CO_2 exchange in controlling the seasonal signal of atmospheric CO_2 at the monitoring stations. To evaluate these relative contributions, we ran the model with each of the different source components separately. In order to separate effects of the middle and high latitudes versus the tropics, we also performed an atmospheric transport model simulation with the SDBM1 fluxes from the latitudes north of 30°N, 30°S-30°N, and south of 30°S only.

Plate 1 shows the relative contributions to the seasonal signal of CO_2 at nine monitoring stations that occur at different latitudes: Alert (ALT, 83°N); Shemya Island (SHM, 53°N); Midway (MID, 28°N); Cape Kumukahi (KUM, 20°N); Christmas Island (CHR, 2°N); Samoa (SMO, 14°S); Amsterdam Island (AMS, 38°S); Palmer Station (PSA, 65°S); and south pole (SPO, 90°S). At the three northernmost stations (ALT, SHM, and MID) the seasonal signal of atmospheric CO_2 is controlled almost entirely by CO_2 exchange of the terrestrial biosphere north of 30°N; fossil fuel emissions, oceanic exchange, and terrestrial exchange south of 30°N have little effect on the seasonal dynamics of atmospheric CO_2. The exchange of CO_2 between the atmosphere and the northern terrestrial biosphere plays a large role in the seasonal dynamics of CO_2 at northern stations because much of the global land mass lies north of 30°N (43%, excluding Antarctica) and NEP is highly seasonal in this region. The effect of the exchange is so strong that the peak-to-peak amplitude measured at northern stations varies between approximately 8 ppmv and 12 ppmv, with greater amplitude at more northern stations.

The control of the terrestrial biosphere on the seasonal signal of stations in the tropics diminishes from north to south (Plate 1). At Cape Kumukahi, which is located in the northern tropics, the seasonal signal of CO_2 is controlled almost entirely by exchange be-

Table 2. Stations From the NOAA Station Network [*Conway et al.*, 1994b] Selected for the Present Study

Station Code	Station	Country	Latitude	Longitude	Elevation, [m]
		Northern Stations			
ALT	Alert, North West Territories	Canada	82°27'N	62°31'W	210
MBC	Mould Bay, North West Territorie.	Canada	76°14'N	119°20'W	15
KTL	Kotelny Island, Siberia	Russia	76°06'N	137°36'E	5
BRW*	Point Barrow, Alaska	United States	71°19'N	156°36'W	11
STM*	Ocean Station M	Norway	66°00'N	2°00'E	6
CBA*	Cold Bay, Alaska	United States	55°12'N	162°43'W	25
SHM	Shemya Island	United States	52°43'N	174°06'E	40
CMO	Cape Meares, Oregon	United States	45°29'N	124°00'W	30
NWR	Niwot Ridge, Colorado	United States	40°03'N	105°38'W	3749
AZR*	Azores (Terceira Island)	Portugal	38°45'N	27°05'W	30
MID	Sand Island, Midway	United States	28°13'N	177°22'W	4
KEY	Key Biscayne, Florida	United States	24°40'N	80°12'W	3
		Tropical Stations			
MLO	Mauna Loa, Hawaii	United States	19°32'N	155°35'W	3397
KUM*	Cape Kumukahi, Hawaii	United States	19°31'N	154°49'W	3
AVI	St. Croix, Virgin Islands	United States	17°45'N	64°45 W	3
GMI	Guam	United States Territory	13°26'N	144°47'E	2
RPB	Ragged Point	Barbados	13°10'N	59°26'W	3
CHR	Christmas Island	Kiribati	2°00'N	157°19'W	3
SEY	Seychelles (Mahe Island)	Seychelles	4°40'S	55°10'E	3
ASC	Ascension Island	United Kingdom	7°55'S	14°25'W	54
SMO	American Samoa	United States Territory	14°15'S	170°34'W	30
		Southern Stations			
AMS	Amsterdam Island	France	37°57'S	77°32'E	150
CGO	Cape Grim, Tasmania	Australia	40°41'S	144°41'E	94
PSA	Palmer Station (Anvers Island)	Antarctica	64°55'S	64°00'W	10
SYO	Syowa Station	Antarctica	69°00'S	39°35'E	11
HBA	Halley Bay	Antarctica	75°40'S	25°30'W	10
SPO	Amundsen Scott (South Pole)	Antarctica	89°59'S	24°48'W	2810

*Stations used to calibrate the diagnostic model SDBM1.

tween the atmosphere and the northern terrestrial biosphere. Close to the equator, the seasonal signal of CO_2 at Christmas Island is still dominated by terrestrial exchanges, although seasonal variations in atmospheric transport induce a substantial seasonal signal from the fossil fuel source [*Heimann et al.*, 1989]. In contrast, the seasonal signal at Samoa, which is located in the southern tropics, is controlled approximately equally by fossil fuel emissions and oceanic exchange and northern terrestrial exchange, the latter now shows a 6-month phase shift leading to a relative maximum in August; tropical and southern terrestrial exchange has little effect on seasonal dynamics of atmospheric CO_2 at this station. Although much of the global land mass occurs between latitudes 30°N and 30°S (45%), the SDBM1 simulation indicates that NEP is highly aseasonal in the tropics, so that the northern terrestrial biosphere exchange still plays a role in the northern tropics but has little effect in the southern tropics. The diminishing role, from north to south, of the atmospheric exchange with northern terrestrial biosphere in controlling the seasonal signal of CO_2 in the tropics is also reflected in the peak-to-peak amplitude, which is approximately 8 ppmv at Cape Kumukahi, 4 ppmv at Christmas Island, and 2 ppmv at Samoa.

At the three southernmost stations (AMS, PSA, and SPO) the seasonal signal of CO_2 is largely controlled by the difference between oceanic exchange and the combination of terrestrial exchange and fossil fuel emissions (Plate 1). Oceanic exchange of CO_2 with the atmosphere is important in the southern latitudes be-

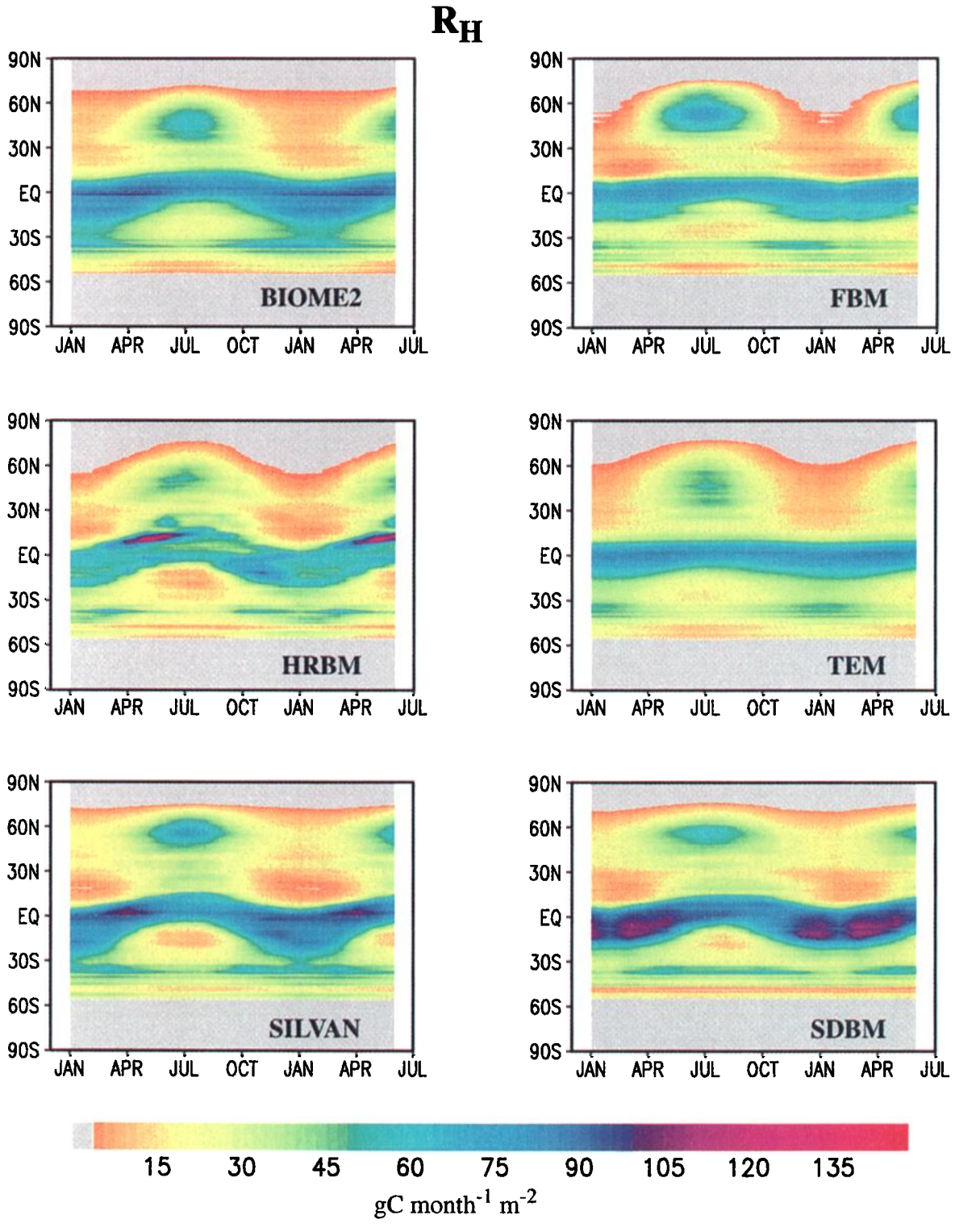

Plate 3c. As in Plate 3a but for heterotrophic respiration (R_H).

Table 3. Mean Squared Deviation Between Observed and Simulated Seasonal Cycle, Normalized by Estimated Standard Deviations of Observations (Equation (15))

	BIOME2	FBM	HRBM	SILVAN	TEM	SDBM1
ALT	44.5	15.5	55.9	7.4	18.6	2.7
MBC	24.0	10.9	31.7	3.9	12.8	2.3
KTL	5.4	3.7	9.6	0.5	2.0	1.7
BRW	20.5	7.5	23.3	4.5	10.0	3.7
STM	25.7	11.2	27.7	14.8	12.2	5.2
CBA	13.0	9.8	15.6	10.2	6.7	4.9
SHM	13.0	9.3	16.0	12.0	5.2	5.6
CMO	15.2	6.9	62.7	1.1	6.9	2.8
NWR	7.1	4.7	5.5	9.6	2.5	1.6
AZR	4.5	2.7	4.6	6.8	1.6	0.5
MID	12.9	7.6	11.7	9.7	2.2	1.2
KEY	11.0	5.5	4.2	23.3	4.4	2.3
MLO	19.0	6.6	11.3	22.8	2.7	2.2
KUM	20.5	10.5	15.0	23.5	4.2	3.6
AVI	5.3	2.2	1.6	19.9	2.0	1.7
GMI	4.6	1.3	3.1	4.1	2.0	0.7
RPB	6.7	6.6	2.0	19.9	26.4	2.0
CHR	4.0	7.5	1.1	4.3	4.0	0.6
SEY	0.6	0.8	0.5	2.1	1.0	0.6
ASC	4.5	8.5	4.7	22.5	13.0	1.3
SMO	1.5	6.4	2.4	5.1	10.4	0.8
AMS	0.3	2.2	0.8	2.9	2.1	0.3
CGO	14.7	7.5	4.9	35.0	24.7	8.4
PSA	12.5	10.9	2.6	41.6	19.1	0.9
SYO	6.9	7.6	3.1	19.0	10.8	0.9
HBA	3.1	6.1	1.5	10.0	9.6	0.3
SPO	23.9	27.3	8.1	73.6	40.6	1.4
			All Stations			
Median	11.0	7.5	4.9	10.0	6.7	1.7
Minimum	0.3	0.8	0.5	0.5	1.0	0.3
Maximum	44.5	27.3	62.7	73.6	40.6	8.4
			Twelve Northern Stations (ALT - KEY)			
Median	13.0	7.6	15.8	8.5	6.0	2.5
Minimum	0.3	0.8	0.5	0.5	1.0	0.3
Maximum	44.5	15.5	62.7	23.3	18.6	5.6
			Nine Tropical Stations (MLO - SMO)			
Median	4.6	6.6	2.4	19.9	4.0	1.3
Minimum	0.6	0.8	0.5	2.1	1.0	0.6
Maximum	20.5	10.5	15.0	23.5	26.4	3.6
			Six Southern Stations (AMS - SPO)			
Median	9.7	7.6	2.8	27.0	14.9	0.9
Minimum	0.3	2.2	0.8	2.9	2.1	0.3
Maximum	23.9	27.3	8.1	73.6	40.6	8.4

cause most of the southern hemisphere is covered by water and little of the global land mass occurs south of 30°S (12%). The effects of terrestrial exchange and fossil fuel emissions on the seasonal signal of CO_2, although small in southern latitudes, are generally in phase with each other and out of phase with the effects of oceanic exchange. Even at the south pole the biospheric signals from the northern, tropical, and southern regions are of similar magnitude and are in phase, such that the total biospheric signal is of the same size as the oceanic signal. Because the effects of oceanic exchange tend to cancel the effects of terrestrial exchange and fossil fuel emissions, the peak-to-peak amplitude of CO_2 at southern stations is less than 2 ppmv.

The fact that in the southern hemisphere south of 30°S the oceanic contribution to the seasonal signal is of similar magnitude as the terrestrial contributions makes these locations less suited as validation sites for the modeled seasonal terrestrial CO_2 exchanges. Pending accurate techniques to separate the terrestrial from the oceanic signals in the observations (e.g., concurrent $^{13}C/^{12}C$ or O_2/N_2 measurements), any discrepancy between simulation and observation could equally well be ascribed to errors in terrestrial or oceanic (or a combination of both) exchange formulations. The main constraint provided by the stations south of 30°S is a bound on the seasonal amplitude which must be smaller than about 2 ppmv (peak to peak) [*Knorr and Heimann*, 1995].

4.2. Comparisons to CO_2 Monitoring Stations: The Five Prognostic TBMs

Estimates of annual NPP and of annual R_H for the terrestrial biosphere by the five prognostic TBMs in this study range from 46.4 Pg C to 61.0 Pg C (FBM, 50.3; HRBM, 46.4; BIOME2 56.6; SILVAN, 61.0; TEM, 49.0; see Table 1). Because controls of the seasonal signal of CO_2 vary latitudinally, we analyze the performance of the TBMs in simulating the seasonal signal of CO_2 separately for northern, tropical, and southern monitoring stations.

4.2.1. Northern stations. At the twelve monitoring stations that occur between latitudes 83°N and 26°N (ALT, MBC, KTL, BRW, STM, CBA, SHM, CMO, AZR, NWR, MID, and KEY), the simulations of the TBMs generally capture the seasonal placement of winter maxima and summer minima in the atmospheric CO_2 signature (Plate 2a), but the phasing of the seasonal signal differs among models. In comparison to the observed seasonal signal of CO_2 at each station, the HRBM and BIOME2 simulations consistently estimate early drawdown and early recovery of atmospheric CO_2. The TEM simulation tends to estimate early drawdown and early recovery at the four northernmost stations (ALT, MBC, KTL, and BRW) but estimates approximately synchronous drawdown and recovery for the other eight stations. The drawdown of CO_2 estimated by the FBM simulation is approximately synchronous for all the stations, but similar to the TEM simulation, the recovery is early for the four northernmost stations and synchronous for the other eight stations. The SILVAN simulation tends to estimate late drawdown for all stations and late recovery at the eight southernmost stations; the recovery at the four northernmost stations is approximately synchronous. All of the simulations tend to underestimate the magnitude of the drawdown for the northern stations, with the HRBM and BIOME2 simulations generally indicating the greatest degree of underestimation and the SILVAN simulation generally indicating the least amount of underestimation.

On the basis of the NMSD index the simulations differ in their fits to the seasonal signal of CO_2 among the 12 northern stations (Figure 3a; Kruskal-Wallis test, H = 13.8, P = 0.008, and d.f. (degrees of freedom) = 4). Pairwise multiple comparisons (Student-Newman-Keuls, $P < 0.05$) indicate that the fits of the FBM (median is 7.6), SILVAN (median is 8.5), and TEM (median is 6.0) simulations are not statistically different from each other but are statistically different from the fits of the HRBM (median is15.8) and BIOME2 (median is 13.0) simulations; the fits of the HRBM and BIOME2 simulations are statistically indistinguishable.

4.2.2. Tropical stations. Nine monitoring stations occur in the tropics between latitudes 20°N and 14°S (Plate 2b; MLO, KUM, GMI, AVI, RPB, CHR, SEY, ASC, and SMO). Three of the stations occur in the northern tropical Pacific Ocean (MLO, KUM, and GMI), two occur in the northeast tropical Atlantic Ocean (AVI and RPB), and four occur near or south of the equator (CHR, SEY, ASC, and SMO). At the three Pacific stations in the northern tropics the HRBM and BIOME2 simulations tend to estimate early drawdown and recovery of atmospheric CO_2. In contrast, the SILVAN simulation estimates late drawdown and recovery. The HRBM, BIOME2, and SILVAN simulations tend to underestimate the degree of drawdown at the three sites. Recovery also is underestimated by the three simulations, except for the SILVAN simulation at Guam. For both the FBM and TEM simulations both the timing and the degree of drawdown and recovery are similar to the observed signal.

At the two Atlantic stations in the northern tropics the SILVAN simulation estimates late drawdown and recovery of atmospheric CO_2; the other simulations are more or less synchronous with the observed signal. Both the BIOME2 and SILVAN simulations tend to underestimate the degree of drawdown at both stations. The BIOME2 simulation also underestimates the degree of recovery. In contrast, the TEM simulation tends to overestimate the degree of recovery at both stations and overestimates the degree of drawdown at RPB. The FBM simulation tends to overestimate recovery at RPB. Both the timing and degree of drawdown and recovery of the HRBM simulation are similar to the observed signal at the two stations.

At each of the tropical stations near or south of the equator, the pattern of simulations are unique. At Christmas Island all of the simulations, except for HRBM, tend to estimate early drawdown and early recovery. The SILVAN and TEM simulations tend to overestimate the degree of recovery. At Seychelles all of the simulations, except for SILVAN, tend to estimate synchronous drawdown and recovery in comparison with the observed signal; the SILVAN simulation indicates late drawdown and recovery. The degree of drawdown and recovery is similar to that of the observed signal for all simulations, mostly because at this site the seasonal monsoon circulation generates a large seasonal signal from the fossil fuel source [*Heimann et al.*, 1989]. At Ascension Island all of the simulations estimate late drawdown and late recovery in comparison to the observed signal. The HRBM simulation overpredicts recovery and the FBM, TEM, and SILVAN simulations overestimate the degree of both drawdown and recovery. All TBMs tend to overpredict the observed peak-to-peak variation by a factor of 2. At Samoa the FBM, TEM, and HRBM simulations estimate early drawdown and recovery, while the SILVAN simulation estimates late drawdown and recovery. The FBM, SILVAN, and TEM simulations also overestimate the degree of drawdown and recovery in comparison to the observed signal.

For the tropical stations the median NMSD indices for the simulations range from 2.4 to 19.9 (FBM, 6.6; HRBM, 2.4; BIOME2, 4.6; SILVAN, 19.9; and TEM, 4.0). On the basis of the NMSD in-

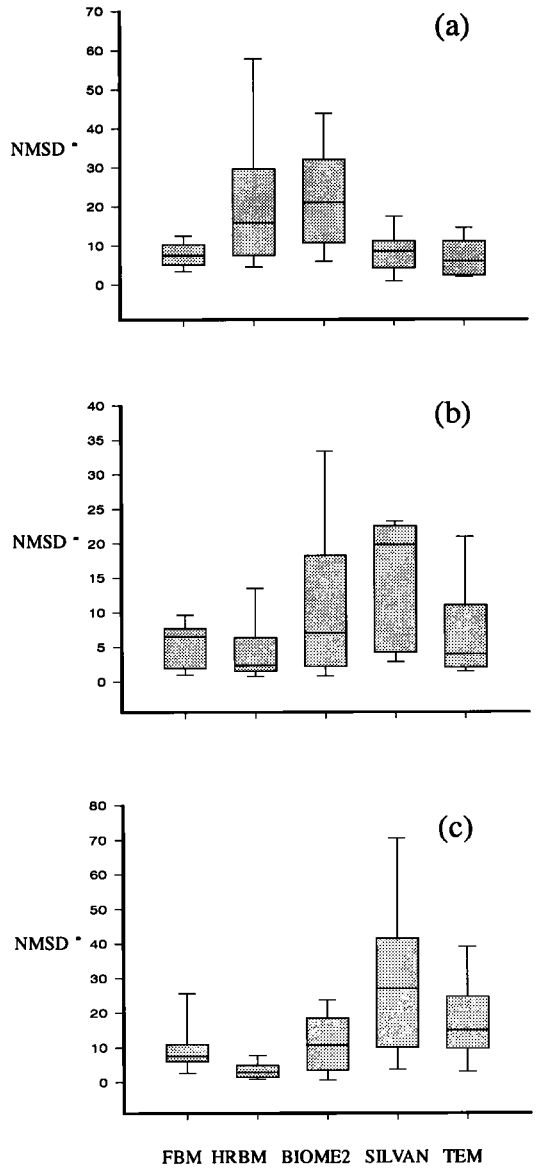

Figure 3. Comparison of the distribution of the normalized mean-squared deviation between the observed seasonal cycle and the simulated seasonal cycle produced by coupling the monthly estimates of net ecosystem production by the prognostic terrestrial biosphere models and fossil fuel emissions with the Hamburg ocean and atmospheric transport models for (a) northern stations, (b) tropical stations, and (c) southern stations. The box plots indicate the median, 25th, and 75th percentile and 10th and 90th percentile intervals.

dex the simulations do not differ in their fits to the seasonal signal of CO_2 among the nine tropical stations (Figure 3b; Kruskal-Wallis test, H = 6.21, P = 0.1841, and d.f. = 4). A power analysis for a one-way analysis of variance indicates that the power to detect differences is low (0.36 versus desired 0.80).

4.2.3. Southern stations. At the six monitoring stations that occur between latitudes 38°S and 90°S (AMS, CGO, SYO, PSA, HBA, and SPO), the simulations of the TBMs do not generally capture the seasonal placement of winter and summer maxima in the atmospheric CO_2 signature (Plate 2c). The BIOME2 and SILVAN simulations are consistently approximately 180° out of phase with the observed seasonal signal at all stations. The other three simulations all estimate late drawdown and recovery in comparison to the observed seasonal signal; the FBM and TEM simulations are approximately in phase with each other and are later than the HRBM simulation. The degree of drawdown and recovery are consistently overestimated by the FBM, SILVAN, and TEM simulations. The degree of drawdown and recovery estimated by the HRBM and BIOME2 simulations are similar to the observed seasonal signal of CO_2 at the six stations.

On the basis of the NMSD index the simulations differ in their fits to the seasonal signal of CO_2 among the six southern stations (Figure 3c; Kruskal-Wallis test, H = 9.51, P = 0.0495, and d.f. = 4). Pairwise multiple comparisons (Student-Newman-Keuls, $P < 0.05$) indicate that fits of the FBM (median is 7.6), BIOME2 (median is 9.7), SILVAN (median is 27.0), and TEM (median is14.9) simulations are not statistically different from each other but are statistically different from the fits of the HRBM simulation (median is 2.8).

4.3. Comparisons of Latitudinal-Seasonal Patterns of NEP: Prognostic TBMs Versus the SDBM1

On the basis of the NMSD index the simulations of the five prognostic TBMs and the SDBM1 differ in their fits to the seasonal signal of CO_2 among the 27 monitoring stations (Figure 4; Kruskal-Wallis test, H = 37.7, $P < 0.0001$, and d.f. = 5). Pairwise multiple comparisons (Student-Newman-Keuls, $P < 0.05$) indicate that the fits of the FBM (median is 7.5), HRBM (median is 4.9),

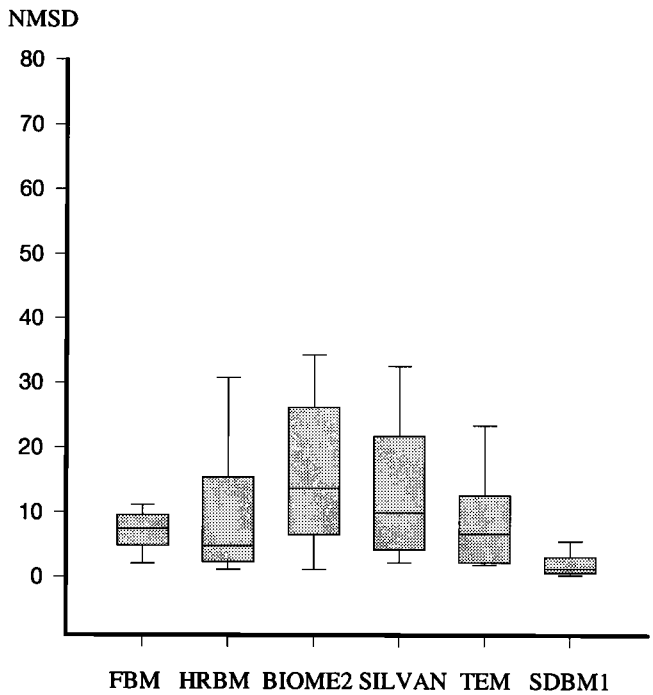

Figure 4. Comparison of the distribution of the normalized mean-squared deviation between the observed seasonal cycle and the simulated seasonal cycle produced by coupling the monthly estimates of net ecosystem production by terrestrial biosphere models and fossil fuel emissions with the Hamburg ocean and atmospheric transport models for all of the 27 monitoring stations. The box plots indicate the median, 25th, and 75th percentile and 10th and 90th percentile intervals.

BIOME2 (median is 11.0), SILVAN (median is 10.0), and TEM (median is 6.7) simulations are not statistically different from each other but are statistically different from the SDBM1 simulation (median is 1.7). The SDBM1 simulation indicates that control of the terrestrial biosphere over the seasonal dynamics of CO_2 in the atmosphere diminishes from north to south and suggests that NEP is highly seasonal in northern regions and highly aseasonal in tropical regions. Because of the singularly close fit of the SDBM1 simulation to the seasonal signature of CO_2 at the monitoring stations, the latitudinal-seasonal pattern of NEP estimated by the SDBM1 is a useful standard for comparison to the other TBMs. However, it is important to keep in mind that the simulations with the SDBM1 do not include CO_2 exchanges caused by land use (e.g., biomass burning).

For northern regions of the terrestrial biosphere, the SDBM1 indicates that NEP is highly seasonal (Plate 3a). All of the five prognostic models also indicate that northern regions are highly seasonal, but the magnitude and timing of CO_2 uptake and release by the terrestrial biosphere differs among the models. The maximum uptake of CO_2 in the northern terrestrial biosphere estimated by FBM, HRBM, and TEM is similar to the maximum uptake estimated by the SDBM1, but the timing of maximum uptake tends to be earlier, and the growing season appears to be shorter in comparison to the SDBM1. The release of CO_2 to the atmosphere estimated by the three models during the winter is less than that estimated by the SDBM1. The timing of maximum uptake of CO_2 estimated by the SILVAN model is later than that of the SDBM1, but the magnitude of uptake appears to be similar. The release of CO_2 estimated by the SILVAN model is similar to that estimated by the SDBM1. In comparison to the SDBM1 the BIOME2 model estimates less release of CO_2 to the atmosphere during winter; the timing of uptake is earlier, and the magnitude of uptake is smaller. Thus, although the estimates of the prognostic models and the SDBM1 agree that NEP in the northern terrestrial biosphere is highly seasonal, the prognostic models differ from the SDBM1 in the magnitude and/or timing of CO_2 exchange with the atmosphere in this region.

For tropical regions of the terrestrial biosphere the SDBM1 indicates that the seasonality of NEP is much less pronounced than in northern regions (Plate 3a). In contrast, the NEP estimates of all five prognostic models are highly seasonal. The maximum uptake of CO_2 in the tropical terrestrial biosphere estimated by the FBM, HRBM, SILVAN, and TEM is greater than the maximum uptake estimated by the SDBM1. The maximum uptake estimated by the BIOME2 model is similar to that of the SDBM1 in the northern tropics but is greater in the southern tropics. All five of the prognostic TBMs estimate substantial release of CO_2 to the atmosphere during the tropical dry season; the estimated releases are most pronounced for the FBM, HRBM, and TEM. In general, seasonality of NPP in the tropics differs more between the prognostic and diagnostic models than does the seasonality of R_H (Plates 3b and 3c).

For southern regions of the terrestrial biosphere, the SDBM1 indicates that NEP is highly seasonal (Plate 3a). All of the prognostic TBMs estimate that the uptake of CO_2 from the atmosphere occurs between October and April, which is generally in agreement with the SDBM1 estimates. The FBM and HRBM estimates indicate higher maximum uptake of CO_2 than the SDBM1 estimates, and the BIOME2, SILVAN, and TEM estimates indicate lower maximum uptake of CO_2. In comparison to the SDBM1 the estimated release of CO_2 to the atmosphere is extended in the FBM and HRBM estimates; the timing and magnitude of CO_2 releases estimated by the other three models are similar to the SDBM1 in the southern portions of the terrestrial biosphere.

5. Discussion and Conclusions

The simulations with the diagnostic model SDBM1, which is tuned to the atmospheric CO_2 seasonal signal at five monitoring stations in the northern hemisphere, successfully reproduced the seasonal signal of CO_2 at the other monitoring stations. The additional simulation experiments with the SDBM1 source split among tropics and extratropical latitudes demonstrate that the seasonal signal both north and within the tropics is dominated by the exchanges with the terrestrial biosphere. In southern latitudes, however, ocean-atmosphere gas exchange contributes significantly to the seasonal signal of CO_2.

Among the 27 monitoring stations the NMSD (equation (15)) of the SDBM1 simulation was greater than 5 at only four of the stations (Station M, Cold Bay, Shemya, and Cape Grim). Several aspects of the methodology of the present study may be responsible for the differences. First, there is uncertainty as to how well the atmospheric tracer transport model (TM2) performs at high northern latitudes. Poor performance of TM2 at northern latitudes might explain the poorer fits at Station M, Cold Bay, and Shemya. Second, our assumption of time invariant fossil fuel emissions may be inaccurate. For instance, *Levin et al.* [1989] found that the seasonality of the fossil fuel flux from Europe is about 3 times higher than the seasonality estimated from emission statistics. This might contribute to the seasonal signal observed at Station M. Third, errors in the simulated ocean exchange with the atmosphere may become important in the southern hemisphere. It should also be recognized that we have not included in our analyses biomass burning nor the global terrestrial sink which can be inferred from the global budget of atmospheric CO_2 [*Schimel et al.*, 1995]. Some noticeable effects from tropical vegetation fires may be expected at AVI, RPB, and ASC according to a study by *Iacobellis et al.* [1994]. Vegetation fires in the tropics and subtropics are expected to occur primarily during the dry season when NPP is reduced because of water stress. Hence if vegetation fires make up for a significant atmospheric signal in atmospheric CO_2, then our analysis, which neglected this additional flux, should result in an underestimation of the amplitude of the seasonal signal. These additional effects are difficult to quantify, however, because of an uncertain database on the CO_2 release from vegetation fires and the subsequent uptake by regrowing vegetation. Another explanation for differences may be the use of 1987 wind fields in TM2 which may not be representative for the entire period of CO_2 measurements (1983-1992); in a sensitivity study, *Knorr and Heimann* [1995, Table 2] documented a 15% change in the overall agreement when using wind data from 1986. Finally, because we compare model output of TM2 at approximately 7.83° by 10° resolution with point station measurements, we potentially neglect the influence of local sources.

There are several aspects of the SDBM1 extrapolations for NPP and R_H that may influence the fit between the SDBM1 simulations and the observations. First, the use of constant global light use efficiency and Q_{10} values is clearly an oversimplification [*Ruimy et al.*,1994]. Also, the use of monthly maximum NDVI from a 5-year period in the SDBM simulations may not be representative for the entire period of CO_2 measurements. Finally, because the SDBM1 calculates fluxes at monthly temporal resolution, there may be

phase differences of up to two 2 between simulated and observed signals.

Even though there are a number of concerns that could influence the fit of the SDBM1 simulations with the observed seasonal signal of atmospheric CO_2, the simulation with the diagnostic model significantly fits the seasonal signal better than any of the simulations with the prognostic TBMs. Only at Cape Grim did simulations with prognostic TBMs produce smaller NMSD values than the SDBM1 simulation (see Table 3), which, however, may be a coincidence considering the problem of data selection at this site as discussed in section 4.1. The most likely explanation for the different fits to the observed data is the use of phenology algorithms in the prognostic models versus the use of NDVI which essentially defines phenology in the diagnostic model. The variability in phase of the seasonal cycle among simulations with prognostic models is presumably caused by variation in the phenology algorithms of the models. An additional, although minor source of variability among the prognostic TBMs may be due to different vegetation maps and different techniques to interpolate the monthly climate variables to the time resolution of the model. It must also be recognized that the use of NDVI in the diagnostic model implicitly may partially account for the effects of land use on terrestrial CO_2 exchange. In contrast, the prognostic models use potential vegetation hence do not consider land use. However, preliminary sensitivity simulations in which the prognostic models masked out agriculturally used land pixels showed only very small differences in the seasonal cycle at the monitoring stations as compared to the base simulation.

The fits of the prognostic simulations depend on the region of the globe. At the northern stations all models tend to underestimate the seasonal amplitude and, in general, predict early drawdown and recovery. However, the general phasing of the northern hemisphere CO_2 concentration with a minimum in late summer and a maximum in spring is captured by all models. One hypothesis to explain the underestimation of the seasonal amplitude is that all the models predict in high latitudes a too strong seasonality of heterotrophic respiration, which, in these regions, is controlled primarily by the annual cycle of temperature. This defect might be due to the fact that the TBMs implement base metabolic rates of soil decomposition that have no temperature dependence. Emerging data indicate that the base metabolic rate of decomposition above 10°C is much higher than below 10°C (J. M. Melillo, unpublished data 1996; K. J. Nadelhoffer, unpublished data, 1996), that is, there appears to be a threshold temperature for base metabolic rates.

The consistently underestimated seasonal amplitude generated by BIOME2 throughout the entire northern hemisphere stations is attributed in part to a too strong seasonality in heterotrophic respiration which is generated from the *Howard and Howard* [1993] formulation and which hence cancels a too large fraction of the seasonal drawdown of CO_2 by the modeled NPP.

The relatively late drawdown of SILVAN in the northern latitudes results from the maximal NPP being late compared to the other models (Plate 3). In the temperate and boreal biomes the phenology of leaves as a function of the date of the year in SILVAN is determined on the basis of heat sums and not on the basis of potential NPP computed from concurrent climate and vegetation state. This appears to lead to a later bud burst and thus to later NPP simulated by SILVAN than as simulated by the other models in the northern latitudes.

At the tropical and southern stations the differences in the fits of the prognostic and diagnostic models generally become larger from north to south. For example, at Ascension Island (ASC, 7°55'S), located in the tropical Atlantic, all the prognostic models consistently overpredict the observed seasonality, most prominently seen in the large peak appearing during November and December. The seasonal cycle at this station is primarily influenced by seasonal terrestrial CO_2 exchanges in tropical southern Africa and South America [*Kaminski et al.*, 1996].

One hypothesis to explain the overestimation of CO_2 release of the terrestrial biosphere during the dry period in the tropical regions is that none of the TBMs allow tropical trees access to deep soil water. In some regions of the tropics, evergreen forests have been able to maintain evapotranspiration during 5-month dry periods by absorbing water from soil depths of more than 8 m [*Nepstad et al.*, 1994]. The TBMs in this study have rooting zones for tropical forests that range from 1 m to 3 m, depending on the model. The use of NDVI by the SDBM1 to some extent implicitly accounts for the effects of deep rooting on phenology. Furthermore, since in the SDBM1 the same water stress factor is applied on the formulations of NPP and R_H, its effects on the resulting net seasonal CO_2 flux is minimized.

Another hypothesis to explain differences in the latitudinal-seasonal pattern of NEP between the estimates of the prognostic TBMs and the SDBM1 in the tropics is that plant respiration is overestimated by the prognostic TBMs. Uncertainty in respiration budgets occurs because there is poor information on the relative amounts of actively respiring plant tissue (leaves, fine roots, and sapwood) and inactive plant tissue (heartwood and coarse roots).

In SILVAN the delay of the seasonal cycle by approximately 2 months in tropical latitudes appears to be caused by the relatively early reduction of heterotrophic respiration (see Plate 3, compare SILVAN with SDBM) as a result of the reduced precipitation during the dry season. Hence the accumulated litter from the previous growing season tends to be preserved until the onset of the following rainy season, when it is respired, yielding a large pulse which tends to delay the concurrent drawdown of the CO_2 concentration by new production.

It is difficult to attribute the large differences between the fits of the prognostic and diagnostic models in southern regions to particular deficiencies in model formulations or particular problem areas. However, a thorough investigation is not warranted in this region because, as discussed in section 4.1., the northern hemisphere middle and high latitudes, the tropics and the southern hemisphere midlatitudes, and also the ocean component contribute about equally to the seasonal signal. Furthermore, the signals in the southern hemisphere midlatitudes are small and show substantial interannual variations. In the future, high-precision stable isotope data ($^{13}C/^{12}C$) might provide an additional tool to discriminate between the different contributions.

In a similar study, *Hunt et al.* [1996] have used a description of actual vegetation to compare the simulated seasonal signal of CO_2 with the BIOME-BGC model, driven by 1987 weather data [*Piper and Stewart*, 1996], to the measured CO_2 signal for the year 1987. Also, they derived annual maximum LAI from 1987 NDVI data and used this maximum LAI to initialize the carbon and nitrogen pools. In our study we have used potential vegetation to make the comparison of the simulated seasonal signal of each of five prognostic TBMs, driven by a long-term average climate, to the average seasonal signal of the period 1983-1992. Although the nature of the comparisons are somewhat different, the analyses presented here and by *Hunt et al.* [1996] are important for evaluating the dynamics

of global TBMs and for gaining further insight into the biosphere's role in controlling the seasonal signal of atmospheric CO_2 concentration. The differences in the predictions by the five models will be further analyzed by developing a modularized Community Terrestrial Biosphere Model which allows us to combine modules from the different TBMs.

The study forms part of the Electric Power Research Institute Carbon Cycle Model Linkage Project, which is using comprehensive models including terrestrial, oceanic, and atmospheric components to analyze the dynamics of the global carbon cycle during the historical (fossil fuel) and contemporary periods and to examine the response of the carbon cycle to different scenarios of future emissions. In the present analysis, interannual variability and secular trends were factored out so as to test the ability of current TBMs to simulate one specific aspect of the contemporary carbon cycle, that is, the seasonal cycle of CO_2 concentrations in the atmosphere. Simulations with the prognostic TBMs successfully reproduced aspects of the seasonal signal of atmospheric CO_2 which could not be anticipated because these models were not calibrated to the atmospheric CO_2 signal. We consider this demonstration essential to establish the usefulness of TBMs for subsequent analyses in which we will relax the assumption of equilibrium in the terrestrial carbon balance and take into account the physiological effects of CO_2 increase, climate variability, and climate change.

Acknowledgments. We cordially thank Lou Pitelka from the Electric Power Research Institute (EPRI, Palo Alto, California, U.S.A.) for his help and stimulating discussions. We gratefully acknowledge a constructive review by Steve Piper. This study was conducted in part within the Carbon Cycle Model Linkage Project with support by EPRI (RP 3416-01), IGBP-GAIM, and the German Ministry for Education and Research (BMBF). Computing support was provided by the German Climate Computing Center (DKRZ) in Hamburg.

References

Campbell, G.S., *An Introduction to Environmental Biophysics*, Springer, New York, 1997.

Collatz, G. J., J. T. Ball, C. Grivet, and J. A. Berry, Physiological and environmental regulation of stomatal conductance, photosynthesis and transpiration: A model that includes a laminar boundary layer, *Agric. For. Meteorol., 54*, 107-136, 1991.

Collatz, G. J., M. Ribas-Carbo, and J. A. Berry, Coupled photosynthesis-stomatal conductance model for leaves of C_4 plants, *Aust. J. Plant Physiol., 19*, 519-538, 1992.

Conway, T. J., P. Tans, L. S. Waterman, K. W. Thoning, D. R. Buanerkitzis, K. A. Masarie, and N. Zhang, Evidence for interannual variability of the carbon cycle from the NOAA/CMDL global air sampling network, *J. Geophys. Res., 99*, 22831-22855, 1994a.

Conway, T. J., P. P. Tans, and L. S. Waterman, Atmospheric CO_2 from sites in the NOAA/CMDL air sampling network, in *Trends '93: A Compendium of Data on Global Change*, edited by T. A. Boden et al., *Rep. ORNL/CDIAC-65*, pp. 41-119, Carbon Dioxide Inf. Anal. Cent., Oak Ridge Nat. Lab., Oak Ridge, Tenn., 1994b.

Esser, G., Sensitivity of global carbon pools and fluxes to human and potential climate impacts, *Tellus, Ser. B, 39*, 24-60, 1987.

Esser, G., Osnabrück Biosphere Model: Structure, construction, results, in *Modern Ecology - Basic and Applied Aspects*, edited by G. Esser and D. Overdieck, pp. 679-709, Elsevier, New York, 1991.

Esser, G., J. Hoffstadt, F. Mack, and U. Wittenberg, High Resolution Biosphere Model - Documentation, *Mitteil. 2*, Inst. für Pflanzenökol. der Justus-Liebig-Univ. Giessen, Germany, 1994.

Farquhar, G. D., S. von Caemmerer, and J. A. Berry, A biochemical model of photosynthetic CO_2 in leaves of C_3 species, *Planta, 149*, 78-90, 1980.

Federer, C. A., Transpirational supply and demand: Plant, soil and atmospheric effects evaluated by simulation, *Water Resour. Res., 18(2)*, 355-362, 1982.

Foley, J. A., Net primary productivity in the terrestrial biosphere: The application of a global model, *J. Geophys. Res., 99*, 20773-20783, 1994.

Food and Agriculture Organization, *Soil Map of the World*, vols. I-X, scale 1:5,000,000, Food and Agricultural Organization and U. N. Educ., Sci. and Cult. Organ., Paris, France, 1971-1979.

Friend, A. D., PGEN: An integrated model of leaf photosynthesis, transpiration, and conductance, *Ecol. Model., 77*, 233-255, 1995.

Fung, I. Y, K. Prentice, E. Matthews, J. Lerner, and G. Russell, Three-dimensional tracer model study of atmospheric CO_2: Response to seasonal exchanges with the terrestrial biosphere, *J. Geophys. Res., 88*, 1281-1294, 1983.

Fung, I. Y., C. J. Tucker, and K. C. Prentice, Application of advanced very high resolution radiometer vegetation index to study atmosphere-biosphere exchange of CO_2, *J. Geophys. Res., 92*, 2999-3015, 1987.

Gallo, K. P., Experimental global vegetation index from AVHRR utilizing pre-launch calibration, cloud and Sun-angle screening, digital data, Nat. Ocean. and Atmos. Admin., Nat. Geophys. Data Cent., Boulder, Co. 1992.

Haxeltine, A., and I. C. Prentice, A general model for the light-use efficiency of primary production, *Funct. Ecol., 10*, 551-561, 1996.

Haxeltine, A., I. C. Prentice, and I. D. Cresswell, A coupled carbon and water flux model to predict vegetation structure, *J. Veg. Sci.*, 7, 651-666, 1996.

Heimann M., The TM2 tracer model, model description and user manual, *DKRZ Rep. 10*, 47 pp., Ger. Clim. Comput. Cent., Hamburg, 1995.

Heimann M. and C. D. Keeling, A three dimensional model of atmospheric CO_2 transport based on observed winds, 2, Model description and simulated tracer experiments, in *Aspects of Climate Variability in the Pacific and the Western Americas, Geophys. Monogr. Ser.*, vol. 55, edited by D. H. Peterson, pp. 237-275, AGU, Washington, D. C., 1989.

Heimann, M. and P. Monfray, Spatial and temporal variation of the gas exchange coefficient for CO_2, 1, Data analysis and global validation, *Max-Planck-Inst. for Meteorol. Rep. 31*, 29 pp., Max-Planck-Inst. for Meteorol., Hamburg, 1989.

Heimann, M., C. D. Keeling, and C. Tucker, A three dimensional model of atmospheric CO_2 transport based on observed winds, 3, Seasonal cycle and synoptic time scale variations, in *Aspects of Climate Variability in the Pacific and the Western Americas, Geophys. Monogr. Ser.*, vol. 55, edited by D. H. Peterson, pp. 277-303, AGU, Washington, D. C., 1989.

Howard, D. M., and P. J. A. Howard, Relationships between CO_2 evolution, moisture content, and temperature for a range of soil types, in *The Global Carbon Cycle and Its Pertubation by Man and Climate, Rep. EPOC-CT90-0017 (MNLA)*, European Union, Brussels, Belgium, 1993.

Hunt, E. R., S. C. Piper, R. Nemani, C. D. Keeling, R. D. Otto, and S. W. Running, Global net carbon exchange and intra-annual atmospheric CO_2 concentrations predicted by an ecosystem process model and three-dimensional atmospheric transport model, *Global Biogeochem. Cycles, 10*, 431-456, 1996.

Iacobellis, S. F., R. Frouin, H. Razafimpanilo, R. C. J. Somerville, and S. C. Piper, North African savanna fires and atmospheric carbon dioxide, *J. Geophys. Res., 99*, 8321-8334, 1994.

Janecek, A., G. Benderoth, M. K. B. Lüdeke, J. Kindermann, and G. H. Kohlmaier, Model of the seasonal and perennial carbon dynamics in deciduous-type forests controlled by climatic variables, *Ecol. Modell., 49*, 101-124, 1989.

Jensen, M. E., and H. R. Haise, Estimating evapotranspiration from solar radiation, *J. Irrig. Drain. Div., Am. Soc. Civ. Eng., 89(IR4)*, 15-41, 1963.

Joyce, L. A., J. Mills, L. Heath, A. D. McGuire, R. W. Haynes, and R. A. Birdsey, Forest sector impacts from changes in forest productivity under climate change, *J. Biogeogr., 22*, 703-714, 1995.

Kaduk, J., Simulation der Kohlenstoffdynamik der globalen Landbiosphäre mit SILVAN - Modellbeschreibung und Ergebnisse, Ph. D. thesis, 157 pp., Univ. of Hamburg, Hamburg, Germany, July, 1996.

Kaduk, J. and M. Heimann, A prognostic phenology scheme for global models of the terrestrial biosphere, *Clim. Res., 6*, 1-19, 1996.

Kaminski, T., R. Giering, and M. Heimann, Sensitivity of the seasonal cycle of CO_2 at remote monitoring stations with respect to seasonal surface exchange fluxes determined with the adjoint of an atmospheric transport model, *Phys. Chem. Earth, 21*, 457-462, 1996.

Keeling, C. D., R. B. Bacastow, A. F. Carter, S. C. Piper, T. P. Whorf, M. Heimann, W. G. Mook, and H. Roeloffzen, A three dimensional model of atmospheric CO_2 transport based on observed winds, 1, Analysis of observational data. In *Aspects of Climate Variability in the Pacific and the Western Americas, Geophys. Monogr. Ser.*, vol. 55, edited by D. H. Peterson, pp. 165-236, AGU, Washington, D. C., 1989.

Keeling, C. D., T. P. Whorf, M. Wahlen, and J. van der Plicht, Interannual extremes in the growth of atmospheric CO_2, *Nature, 375*, 666-670, 1995.

Kindermann, J., et al., Structure of a global carbon exchange model for the terrestrial biosphere: The Frankfurt Biosphere Model (FBM), *Water Air Soil Pollut., 70*, 675-684, 1993.

Knorr, W., and M. Heimann, Impact of drought stress and other factors on seasonal land biosphere CO_2 exchange studied through an atmospheric tracer transport model, *Tellus Ser. B, 47, 4*, 471-489, 1995.

Kohlmaier, G. H., et al., The Frankfurt Biosphere Model: A global process oriented model for the seasonal and longterm CO_2 exchange between terrestrial ecosystems and the atmosphere, 2, Global results for potential vegetation in an assumed equilibrium state, *Clim. Res., 8*, 61-87, 1997.

Kurz, K. D., Zur saisonalen Variabilität des ozeanischen Kohlendioxidpartialdrucks, Ph. D. thesis, 107 pp., Univ. of Hamburg, Hamburg, Germany, November 1993.

Larcher, W., Physiological Plant Ecology, 303 pp., Springer-Verlag, New York, 1980.

Law, R. M., et al., Variations in modeled atmospheric transport of carbon dioxide and the consequences for CO_2 inversions, *Global Biogeochem. Cycles, 10*, 783-796, 1996.

Leemans, R., and W. P. Cramer, The IIASA database for mean monthly values of temperature, precipitation, and cloudiness on a global terrestrial grid, *Rep. IIASA RR-91-18*, Laxenburg, Int. Inst. Appl. Syst. Anal., Austria, 1991.

Levin, I., J. Schuchard, B. Kromer, and K. O. Münnich, The continental European Suess-effect, *Radiocarbon 32(1)*, 431-440, 1989.

Levin, I., R. Graul, and N. B. A. Trivett, Long-term observations of atmospheric CO_2 and carbon isotopes at continental sites in Germany, *Tellus, Ser. B, 47*, 23-24, 1995.

Lieth, H., Modeling the primary productivity of the world, in *Primary Productivity of the Biosphere*, edited by H. Lieth and R.H. Whittaker, pp. 237-263, Springer-Verlag, New York, 1975.

Liss, P. S., and L. Merlivat, Air-sea gas exchange rates: Introducton and synthesis, in *The Role of Air-Sea Exchange in Geochemical Cycling*, edited by P. Buat-Ménard, pp. 113-127, D. Reidel, Norwell, Mass., 1986.

Lloyd, J., and J. A. Taylor, On the temperature dependence of soil respiration, *Funct. Ecol., 8*, 315-323, 1994.

Lüdeke, M. K. B., et al., The Frankfurt Biosphere Model: A global process oriented model for the seasonal and longterm CO_2 exchange between terrestrial ecosystems and the atmosphere, 1, Model description and illustrating results for the vegetation types cold deciduous and boreal forests, *Clim. Res., 4*, 143-166, 1994.

Lüdeke, M. K. B., S. Dönges, R. D. Otto, J. Kindermann, F.-W. Badeck, P. Ramge, U. Jäkel, and G. H. Kohlmaier, Responses in NPP and carbon stores of the northern biomes to a CO_2-induced climatic change, as evaluated by the Frankfurt Biosphere Model (FBM), *Tellus, Ser. B, 47*, 191-205, 1995.

Lüdeke, M. K. B., P. H. Ramge, and G. H. Kohlmaier, The use of satellite-detected NDVI data for the validation of global vegetation phenology models and application to the Frankfurt Biosphere Model, *Ecol. Modell., 91*, 255-270, 1996.

Lurin, B., W. Cramer, B. Moore III, and S. I. Rasool, Global terrestrial net primary productivity, *Global Change NewsLett. (IGBP), 19*, 6-8, 1994.

Maier-Reimer, E., Geochemical cycles in an ocean general circulation model: Preindustrial tracer distributions, *Global Biogeochem. Cycles, 7*, 645-677, 1993.

Maier-Reimer E., U. Mikolajewicz, and K. Hasselmann, Mean circulation of the Hamburg LSG OGCM and its sensitivity to the thermohaline surface forcing, *J. Phys. Oceanogr., 23*, 731-757, 1993.

Marland, G., T. A. Boden, R. C. Griffin, S. F. Huang, P. Kanciruk and T. R. Nelson, Estimates of CO_2 emissions from fossil fuel burning and cement manufacturing, based on the U. S. Bureau of Mines cement manufacturing data, *Rep. ORNL/CIAC-25, NDP-030*, Carbon Dioxide Inf. Anal. Cent., Oak Ridge Nat. Lab., Oak Ridge, Tenn., 1989.

McGuire, A. D., J. M. Melillo, L. A. Joyce, D. W. Kicklighter, A. L. Grace, B. Moore III, and C. J. Vörösmarty, Interactions between carbon and nitrogen dynamics in estimating net primary productivity for potential vegetation in North America, *Global Biogeochem. Cycles, 6*, 101-124, 1992.

McGuire, A. D., L. A. Joyce, D. W. Kicklighter, J. M. Melillo, G. Esser, and C. J. Vörösmarty, Productivity response of climax temperate forests to elevated temperature and carbon dioxide: A North American comparison between two global models, *Clim. Change, 24*, 287-310, 1993.

McGuire, A. D., J. M. Melillo, D. W. Kicklighter, and L. A. Joyce, Equilibrium responses of soil carbon to climate change: Empirical and process-based estimates, *J. Biogeogr., 22*, 785-796, 1995.

McGuire, A. D., D. W. Kicklighter, and J. M. Melillo, Global climate change and carbon cycling in grasslands and conifer forests, in *Global Change: Effects on Coniferous Forests and Grasslands, SCOPE 56*, edited by A. I. Breymeyer, D. O. Hall, J. M. Melillo, and G. I. Agren, pp. 389-411, John Wiley, New York, 1996.

McGuire, A. D., J. M. Melillo, D. W. Kicklighter, Y. Pan, X. Xiao, J. Helfrich, B. Moore III, C. J. Vorosmarty, and A. L. Schloss, Equilibrium responses of global net primary production and carbon storage to doubled atmospheric carbon dioxide: Sensitivity to changes in vegetation nitrogen concentration, *Global Biogeochem. Cycles, 11*, 173-189, 1997.

McNaughton, K. G., and P. G. Jarvis, Predicting effects of vegetation changes on transpiration and evaporation. In *Water Deficit and Plant Growth*, edited by T. T. Kozlowski, pp. 1-47, Academic Press, New York, 1983.

Melillo, J. M., A. D. McGuire, D. W. Kicklighter, B. Moore III, C. J. Vörösmarty, and A. L. Schloss, Global change and terrestrial net primary production, *Nature, 363*, 234-240, 1993.

Melillo, J. M., D. W. Kicklighter, A. D. McGuire, W. T. Peterjohn, and K. M. Newkirk, Global change and its effects on soil organic carbon stocks, in *Role of Nonliving Organic Matter in the Earth's Carbon Cycle*, edited by R. G. Zepp and C. Sontag, pp. 175-189, John Wiley, New York, 1995.

Monsi, M. and T. Saeki, Über den Lichtfaktor und den Pflanzengesellschaften und seine Bedeutung für die Stoffproduktion, *Jpn. J. of Bot., 14*, 22-52, 1953.

Murray, M. B. , M. G. R. Cannell and R. I. Smith, Date of budburst of fifteen tree species in Britain following climate warming, *J. Appl. Ecol., 26*, 693-700, 1989.

Nepstad, D. C., C. R. de Carvalho, E. A. Davidson, P. H. Jipp, P. A. Lefebvre, G. H. Negreiros, E. D. da Silva, T. A. Stone, S. E. Trumbore, and S. Vieira, The role of deep roots in the hydrological and carbon cycles of Amazonian forests and pastures, *Nature, 372*, 666-669, 1994.

Nevison, C. D., G. Esser, E. A. Holland, A global model of changing N_2O emissions from natural and perturbed soils, *Clim. Change, 32*, 327-378, 1996.

Piper, S. C., and E. F. Stewart, A gridded global data set of daily temperature and precipitation for terrestrial biospheric modeling, *Global Biogeochem. Cycles, 10*, 757-782, 1996.

Potter, C. S., J. T. Randerson, C. B. Field, P. A. Matson, P. M. Vitousek, H. A. Mooney, and S. A. Klooster, Terrestrial ecosystem production: A process model based on global satellite and surface data, *Global Biogeochem. Cycles, 7*, 811-842, 1993.

Prentice, I. C., W. Cramer, S. P. Harrison, R. Leemans, R. A. Monserud, and A. M. Solomon, A global biome model based on plant physiology and dominance, soil properties and climate, *J. of Biogeogr., 19*, 117-134, 1992.

Raich, J. W., E. B. Rastetter, J. M. Melillo, D. W. Kicklighter, P. A. Steudler, B. J. Peterson, A. L. Grace, B. Moore III, and C. J. Vörösmarty, Potential net primary productivity in South America: Application of a global model, *Ecol. Appl., 1*, 399-429, 1991.

Ramonet, M., and P. Monfray, P., Selection of baseline conditions in a 3D atmospheric transport model: application to the seasonal and synoptic variations of CO_2, *Tellus, Ser. B, 48*, 502-520, 1996.

Rastetter, E. B., A. W. King, B. J. Cosby, G. M. Hornberger, R. V. O'Neill, and J. E. Hoppie, Aggregating fine-scale ecological knowledge to model coarser-scale attributes of ecosystems, *Ecol. Appl., 2*, 55-70, 1992.

Rotty, R., Estimates of the seasonal variation in fossil fuel CO_2 emissions, *Tellus, Ser. B, 39*, 203-208, 1987.

Ruimy, A., B. Saugier, and G. Dedieu, Methodology for the estimation of terrestrial net primary production from remotely sensed data, *J. Geophys. Res., 99*, 5263-5283, 1994.

Russell, G., and J. Lerner, A new finite-differencing scheme for the tracer transport equation, *J. Appl. Meteorol., 20*, 1483-1498, 1981.

Schimel, D. S., Terrestrial ecosystems and the carbon cycle, *Global Change Biol., 1*, 77-91, 1995.

Six, K. D., and E. Maier-Reimer, Effects of plankton dynamics on seasonal carbon fluxes in an ocean general circulation model, *Global Biogeochem. Cycles, 10*, 559-583, 1996.

Thornthwaite, C. W., and J. R. Mather, *Instructions and Tables for Computing Potential Evapotranspiration and the Water Balance, Publ. Climatol.*, vol. 10, No. 3, Lab. of Climatol., Drexel Inst. of Technol., Centerton, New Jersey, 1957.

VEMAP Members, Vegetation/ecosystem modeling and analysis project: Comparing biogeography and biogeochemistry models in a study of terrestrial ecosystem responses to climate change and CO_2 doubling, *Global Biogeochem. Cycles, 9*, 407-437, 1995.

Vörösmarty, C. J., B. Moore III, A. L. Grace, M. P. Gildea, J. M. Melillo, B.

J. Peterson, E. B. Rastetter, and P. A. Steudler, Continental scale models of water balance and fluvial transport: An application to South America, *Global Biogeochem. Cycles, 3*, 241-265, 1989.

Warnant, P., L. François, D. Strivay, and J. C. Gérard, CARAIB: A global model of terrestrial biological productivity, *Global Biogeochem. Cycles, 8*, 255-270, 1994.

Woodward, F. I., T. M. Smith, and W. R. Emanuel, A global primary productivity and phytogeography model, *Global Biogeochem. Cycles, 9*, 471-490, 1995.

G. Esser and U. Wittenberg, Institut für Pflanzenökologie, Justus-Liebig-Universität, Heinrich-Buff-Ring 38, D-35392 Giessen, Germany. (e-mail: esser@bombax.bio.uni-giessen.de; Uwe.Wittenberg@bot2.bio.uni-giessen.de)

A. Haxeltine, and I.C. Prentice, Global Systems Group, Department of Ecology University of Lund, Sölvegatan 37, S-223 62 Lund, Sweden. (e-mail: alex@planteco.lu.se; colin@planteco.lu.se)

M. Heimann, W. Knorr, and W. Sauf, Max-Planck-Institut für Meteorologie, Bundesstrasse 55, D-20146 Hamburg, Germany. (e-mail: martin.heimann@dkrz.de; knorr@dkrz.de; sauf@dkrz.de)

J. Kaduk, Department of Plant Biology, Carnegie Institution of Washington, 260 Panama Street, Stanford, CA 94305-1297. (e-mail: joerg@jasper.stanford.edu)

D. W. Kicklighter and J. Melillo, The Ecosystems Center, Marine Biological Laboratory, Woods Hole, MA 02543. (e-mail: dkick@lupine.mbl.edu; jmelillo@lupine.mbl.edu)

G. H. Kohlmaier, R. D. Otto, and G. Würth, Institut für Physikalische und Theoretische Chemie, J. W. Goethe-Universität, Marie-Curie-Strasse 11, D-60439 Frankfurt am Main, Germany. (e-mail: g.kohlmaier@chemie.uni-frankfurt.de; wuerth@chemie.uni-frankfurt.de)

A. D. McGuire, Alaska Cooperative Fish and Wildlife Research Unit, National Biological Service, University of Alaska, Fairbanks AK 99775. (e-mail: ffadm@aurora.alaska.edu)

B. Moore III and A. Schloss, Center for Complex Systems, Institute for the Study of Earth, Oceans, and Space, University of New Hampshire, Durham, NH 03824. (e-mail: b.moore@unh.edu; annette.schloss@unh.edu)

S. Sitch, Potsdam Institute for Climate Impact Research, P.O. Box 60 12 03, D-14412 Potsdam, Germany. (e-mail: sitch@pik-potsdam.de)

(Received July 8, 1966; revised June 16, 1997;
accepted July 2, 1997.)